

# High-order accurate multi-sub-step implicit integration algorithms with dissipation control for second-order hyperbolic problems

Jinze Li<sup>a,b</sup>, Hua Li<sup>b,\*</sup>, Kaiping Yu<sup>a,\*</sup>, Rui Zhao<sup>a</sup>

<sup>a</sup>Department of Astronautic Science and Mechanics, Harbin Institute of Technology, No. 92 West Dazhi Street, Harbin 150001, China

<sup>b</sup>School of Mechanical and Aerospace Engineering, Nanyang Technological University, 50 Nanyang Avenue, 639798, Singapore

## Abstract

This paper develops an implicit family of sub-step integration algorithms, which firstly requires identical effective stiffness matrices and third-order consistency within each sub-step. Consequently, the trapezoidal rule has to be employed in the first sub-step and optimal spectral properties are naturally embedded into the proposed algorithms. The analysis reveals at the first time that the constructed  $s$ -sub-step implicit schemes with  $s \leq 6$  can reach  $s$ th-order accuracy when achieving dissipation control and unconditional stability simultaneously. Hence, only four cost-optimal high-order implicit algorithms corresponding to three, four, five, and six sub-steps are developed. Unlike some published high-order algorithms, four novel methods do not suffer from order reduction for solving forced vibrations. Moreover, the novel methods overcome the defect that the authors' previous high-order algorithms require an additional solution to obtain accurate accelerations. Linear and nonlinear examples are solved to confirm the numerical performance and superiority of four novel high-order algorithms.

**Keywords:** implicit time integration, composite multi-sub-step, dissipation control, optimal spectral features, high-order accuracy

## 1. Introduction

The numerical simulation of dynamic structures is one of the central problems in computational dynamics. In the past decades, a great number of numerical techniques have been proposed to solve various dynamical problems. When considering linear elastic structures and after using the spatial discretizations [1], the following second-order differential equations of motion can be obtained as

$$\mathbf{M}\ddot{\mathbf{U}}(t) + \mathbf{C}\dot{\mathbf{U}}(t) + \mathbf{K}\mathbf{U}(t) = \mathbf{F}(t) \quad (1)$$

with the appropriate initial conditions  $\mathbf{U}_0 = \mathbf{U}(t_0)$  and  $\dot{\mathbf{U}}_0 = \dot{\mathbf{U}}(t_0)$ . In Eq. (1),  $\mathbf{U}(t)$  collects unknown nodal displacements and a dot denotes differentiation with respect to time  $t$ ;  $\mathbf{M}$ ,  $\mathbf{C}$ , and  $\mathbf{K}$  are the global mass, damping, and stiffness matrices, respectively, and  $\mathbf{F}(t)$  stands for the load vector, as a known function of time  $t$ . Among all numerical techniques to solve the system (1), the preferred one is of the single-step type consisting of updating the displacement, velocity, and acceleration vectors at current time  $t_n$  to the next instant  $t_{n+1} = t_n + \Delta t$ , where  $\Delta t$  denotes the time increment. This type is often called direct time integration algorithms [1], or step-by-step time marching schemes. In

\*Corresponding authors

Email addresses: pinkie.1jz@gmail.com (Jinze Li), 1ihua@ntu.edu.sg (Hua Li), kaipingyu1968@gmail.com (Kaiping Yu), ruizhao@hit.edu.cn (Rui Zhao)

general, according to the computational efficiency, time integration algorithms can be further divided into two parts: explicit and implicit methods, and they possess own advantages and disadvantages. Explicit methods can significantly save the computational cost but only achieve conditional stability, so the used integration steps are strongly limited by their stability limits. The single-step explicit scheme [2] and the composite two-sub-step explicit algorithms [3, 4] are recommended in this paper. These explicit methods all achieve, at least, second-order of accuracy and flexible dissipation control at the bifurcation point, and they are superior to the earlier explicit algorithms. On the other hand, implicit methods need the direct/iterative solver to solve the resulting linearized equations and importantly can achieve unconditional stability, so the used integration steps are often chosen based on the accuracy instead of the stability. The main attention of this paper is paid to developing implicit algorithms.

Many of implicit integration schemes have been developed by using various design ideas. Some well-known implicit algorithms are the Newmark [5], Wilson- $\theta$  [6], HHT- $\alpha$  [7], WBZ- $\alpha$  [8], and generalized- $\alpha$  [9, 10] algorithms. These mentioned algorithms are single-step schemes, so they often achieve second-order accuracy, unconditional stability, the solution of linear systems once within each time step, and self-starting features. It should be emphasized that these algorithms all suffer from unexpected overshoots in displacement and/or velocity when imposing numerical dissipation in the high-frequency range. These algorithms are reduced to either the trapezoidal rule [1] or the midpoint rule in the non-dissipative case. In fact, among all single-step implicit schemes without subsidiary variables, only the trapezoidal rule and the midpoint rule are highly recommended since they possess desired numerical properties.

Recently, some novel implicit integration methods, namely the so-called composite sub-step algorithms, have attracted the attention of some researchers. A composite two-sub-step algorithm was developed by Bathe [11, 12] to successfully solve the strongly nonlinear problems that the non-dissipative trapezoidal rule fails to solve. The Bathe algorithm uses the composite two-sub-step technique. Firstly, the current integration interval  $t \in [t_n, t_{n+1}]$  is split into two sub-intervals  $[t_n, t_n + \gamma \Delta t]$  and  $[t_n + \gamma \Delta t, t_{n+1}]$ , where  $\gamma$  denotes the splitting ratio of sub-step size. Then, the non-dissipative trapezoidal rule [1] and the three-point backward difference formula are used in the first and second sub-steps, respectively. Finally, the resulting scheme achieves the L-stability, second-order accuracy, non-overshooting, and self-starting features. The unique free-parameter  $\gamma$  adjusts numerical dissipation imposed in the low-frequency range. It has been shown in [13, 14] that the Bathe algorithm [11, 12] corresponds to the non-dissipative trapezoidal rule [1] in either  $\gamma = 0$  or 1, while the first-order backward Euler scheme is covered in  $\gamma = 2$ . These facts also explain the reason why  $\gamma$  can adjust numerical dissipation in the low-frequency range. When the parameter  $\gamma$  gets close to either 0 or 1, the numerical behavior of the Bathe algorithm [11, 12] naturally tends to that of the non-dissipative trapezoidal rule, so controlling dissipation in the low-frequency range.

Later, the composite multi-sub-step implicit algorithms using the non-dissipative trapezoidal rule and more general multi-point backward difference scheme have been constructed and analyzed in the literature [15–18]. Besides, other integration algorithms without adopting the trapezoidal rule in the first sub-step have been successfully developed in [19–22] and they predict more accurate solutions for solving some dynamical problems. Two and three sub-steps have been widely used to construct the composite multi-sub-step algorithms since these sub-step schemes can be readily derived and analyzed. For examples, another two Bathe algorithms, named as  $\rho_\infty$ -Bathe [15] and  $\beta_1/\beta_2$ -Bathe [23], are the composite two-sub-step schemes, and they actually share the completely same algorithm structure [14]. The theoretical analysis [14] has shown that the second-order  $\beta_1/\beta_2$ -Bathe algorithm is algebraically identical to the  $\rho_\infty$ -Bathe algorithm, and the first-order  $\beta_1/\beta_2$ -Bathe algorithm is not competitive with other higher-

order composite multi-sub-step methods. The studies have clearly shown that the composite multi-sub-step implicit algorithms attain optimal spectral properties, namely the maximum numerical dissipation but the minimum relative period errors, when achieving identical effective stiffness matrices within each sub-step. Hence, the optimal composite two-sub-step implicit algorithm achieving dissipation control, second-order accuracy, and no overshoots has been proposed in [18]. Other composite two-sub-step schemes, such as  $\rho_\infty$ -Bathe [15], can cover it when achieving optimal spectral properties. Similarly, an optimal three-sub-step implicit method has been also considered in [16], where identical effective stiffness matrices and controllable algorithmic dissipation in the high-frequency range are achieved. It should be pointed out that another composite three-sub-step implicit algorithm [24] is algebraically identical to the earlier published composite scheme [16]. All composite multi-sub-step implicit algorithms mentioned above are only second-order accurate.

High-order accurate integration algorithms often require much more computational cost than the common second-order ones. So far, there have been a great number of studies [25–36] reporting high-order accurate integration algorithms. A preferred way to develop high-order schemes is to operate the first-order differential systems by converting the original second-order equations of motion. The studies [25, 27, 30, 32, 33] used the time finite elements and the weighted residual approach to address the resulting first-order systems. These high-order schemes suffer mainly from two drawbacks. One is that the resulting integration algorithms cannot output acceleration responses, although they are directly self-starting. Moreover, for solving structures subjected to the external loads, the lack of external load analysis could cause the order reduction in displacement and velocity. For example, the third-order and fourth-order accurate schemes [25] from the extrapolated Galerkin time finite elements are only of second-order for solving forced vibrations. The other is how to compute external loads effectively and accurately. Because the load terms are often expressed as the integral form in the current time interval, how to compute these loads in the integral form is crucial to maintain the expected order of accuracy. It is a known fact [28, 36, 37] that the  $(p+1)$ th-order approximation for the second-order dynamical problems imposes  $p$  unknown variables, and thus the order of accuracy can be optimized up to  $(2p-1)$  and  $2p$ . In general, the developed high-order algorithms can be designed to have controllable dissipation capability. The high-order methods are generally  $(2p-1)$ th- and  $2p$ th-order accurate in the dissipative and non-dissipative cases, respectively. It should be emphasized that the high-order methods derived from the transformed first-order systems have to solve the equation system of dimension  $pd \times pd$  where  $p$  and  $d$  denote the number of the involved variables and the degree-of-freedom of the spatially discretized model, respectively. In the work [36], the  $p$ th-order Lagrange polynomial and Gauss-Lobatto integration points are used to develop  $(2p-1)$ th- and  $2p$ th-order accurate algorithms, and a family [28] of high-order algorithms considers  $p$ th-order Hermite interpolation polynomials and higher-order time derivatives of the equilibrium equations. Note that these families [28, 36] of high-order algorithms must solve the equation systems with higher dimensions per time step, so increasing computational costs. It should be pointed out that the effective stiffness matrices of these two methods [28, 36] are neither symmetric nor sparse. Some existing high-order implicit methods [30, 32, 38–40] suffer from these issues. Hence, some researchers [32, 36, 41] proposed various iterative solvers to solve the resulting higher-dimensional equation systems. A recent overview of these high-order implicit algorithms can refer to the literature [37].

On the other hand, high-order integration algorithms [26, 34, 35] directly operating the second-order differential systems show some advantages over other high-order ones, but there are some shortcomings. One of the main advantages of these high-order implicit methods is avoiding solving higher dimensional equation systems per time

step, so significantly reducing computational costs. For instance, the Tarnow and Simo technique [26] is often applied to the single-step non-dissipative schemes, such as the trapezoidal rule and the midpoint rule. When some single-step dissipative schemes are used in the Tarnow and Simo technique, there is the order reduction for the resulting methods. Hence, the high-order schemes from the Tarnow and Simo technique are generally non-dissipative. If the Tarnow and Simo technique is applied to the midpoint rule, the resulting scheme also covers a directly self-starting, fourth-order accurate, and non-dissipative method [42]. A single-step high-order implicit method based on Padé expansion was developed in [43]. The developed method [43] is always non-dissipative due to the use of diagonal Padé approximation, and it involves the complicated calculations of external loads and complex operations. Soares developed a directly self-starting fourth-order integration scheme [44] for solving undamped models. It is reduced to be third- and second-order accurate for numerically and physically damped models, respectively. However, it is only conditionally stable, so its effective applications may be limited. Zhang et al. [34] adopted the composite sub-step technique to develop an implicit family of high-order algorithms with controllable numerical high-frequency dissipation and acceptable computational cost, but these algorithms also present lower-order of accuracy for solving forced vibrations [35]. The second-order accurate  $\rho_\infty$ -Bathe algorithm [15] is reanalyzed to achieve third-order accuracy [45] via considering optimal load selections. The resulting third-order scheme [45, 46] cannot achieve a full range of numerical dissipation and the load information in the previous time step has to be used in the current step. The  $\rho_\infty$ -Bathe method has been revisited [46] to analyze the influence of the time splitting ratio  $\gamma$  on the accuracy. When a complex-valued  $\gamma$  is adopted, the  $\rho_\infty$ -Bathe method can achieve a full range of dissipation control and the fourth-order accuracy is obtained in the non-dissipative case. Adopting the composite sub-step technique, the authors have already developed an implicit family [35] of high-order algorithms. The developed algorithms are directly self-starting, avoiding both calling any starting procedures and computing the initial acceleration vector. In general, the composite  $s$ -sub-step implicit methods [35] with directly self-starting feature can achieve  $s$ th-order accuracy, unconditional stability, no overshoots, and controllable high-frequency dissipation. As stressed by the original study [35], the directly self-starting high-order algorithms require using the equations of motion once additionally to guarantee identical  $s$ th-order accuracy. Otherwise, the methods [35] cannot output the same acceleration accuracy as those in displacement and velocity, which is the common issue encountered by all directly self-starting high-order methods. Following the same analysis technique as [35], the authors will construct and develop a novel implicit family of high-order algorithms to overcome this issue.

Notice that the reviewed high-order implicit methods [26, 34, 35, 42–45] only require solving the equation system of the same dimension as the original equilibrium equations per time step, so the resulting effective stiffness matrix inherits all desired properties of the global mass, damping, and stiffness matrices, such as sparsity, symmetry, and positive definiteness. Therefore, the present study focuses mainly on developing this type of high-order implicit methods. To this end, this paper will design an implicit family of composite multi-sub-step algorithms to achieve

- (a) self-starting property, avoiding imposing an additional starting procedure;
- (b) unconditional stability, making the used integration step limited by the accuracy instead of the stability;
- (c) identical effective stiffness matrices within each sub-step independent of any algorithmic parameters, embedding optimal spectral properties;
- (d) controllable numerical dissipation in the high-frequency range, suppressing spurious high-frequency compo-

nents;

- (e) higher-order accuracy in displacement, velocity, and acceleration for solving general structures, and
- (f) a good balance between computational cost and high-order accuracy. Dimension of the resulting linearized equations is the same as that of the original second-order differential systems when achieving the high-order accuracy.

The remainder of this work is organized as follows. A novel composite  $s$ -sub-step implicit scheme is constructed in Section 2, where the conditions achieving  $p$ th-order accuracy and controllable numerical dissipation are derived. According to these conditions, four novel high-order implicit algorithms are developed in Section 3. Spectral analysis and comparisons with the existing high-order algorithms are given in Section 4, where the unconditional stability and dissipation control are confirmed well for the proposed high-order algorithms. Numerical examples are solved in Section 5 to validate the numerical performance and superiority of four novel high-order schemes. Finally, some important conclusions are summarized in Section 6.

## 2. Development and analysis

This section will firstly present a novel composite  $s$ -sub-step implicit algorithm with undetermined algorithmic parameters to solve the system (1). Then, the conditions achieving the designed order of accuracy are derived by analyzing a damped single-degree-of-freedom (SDOF) system subjected to the external load. The section ends up with the controllable dissipation analysis in the high-frequency range.

### 2.1. The novel $s$ -sub-step implicit algorithm

For the sake of simplify and clarity, the constructed composite  $s$ -sub-step implicit algorithm is described by solving the linear second-order equations of motion (1). Considering the current integration internal  $t \in [t_n, t_n + \Delta t]$ , the composite sub-step technique firstly divides the whole time increment into  $s$  sub-intervals  $\cup_{i=1}^s [t_n + \gamma_{i-1} \Delta t, t_n + \gamma_i \Delta t]$ , where  $\gamma_i$  denotes the splitting ratio of the  $i$ th sub-step. In this paper,  $\gamma_0 = 0$  and  $\gamma_s = 1$  are always used to provide the acceleration responses. Then, an integration scheme in each sub-step  $t \in [t_n + \gamma_{i-1} \Delta t, t_n + \gamma_i \Delta t]$  ( $i = 1, \dots, s$ ) is constructed as

$$\mathbf{M}\ddot{\mathbf{U}}_{n+\gamma_i} + \mathbf{C}\dot{\mathbf{U}}_{n+\gamma_i} + \mathbf{K}\mathbf{U}_{n+\gamma_i} = \mathbf{F}(t_n + \gamma_i \Delta t) \quad (2a)$$

$$\mathbf{U}_{n+\gamma_i} = \mathbf{U}_n + \Delta t \sum_{j=0}^i \alpha_{ij} \dot{\mathbf{U}}_{n+\gamma_j} \quad (2b)$$

$$\dot{\mathbf{U}}_{n+\gamma_i} = \dot{\mathbf{U}}_n + \Delta t \sum_{j=0}^i \alpha_{ij} \ddot{\mathbf{U}}_{n+\gamma_j}. \quad (2c)$$

Notice that numerical solutions ( $\mathbf{U}_{n+1}$ ,  $\dot{\mathbf{U}}_{n+1}$ , and  $\ddot{\mathbf{U}}_{n+1}$ ) at time  $t_{n+1}$  are obtained in the final sub-step  $t \in [t_n + \gamma_{s-1} \Delta t, t_n + \gamma_s \Delta t]$  due to  $\gamma_s = 1$ . That is,

$$\mathbf{M}\ddot{\mathbf{U}}_{n+1} + \mathbf{C}\dot{\mathbf{U}}_{n+1} + \mathbf{K}\mathbf{U}_{n+1} = \mathbf{F}(t_{n+1}) \quad (3a)$$

$$\mathbf{U}_{n+1} = \mathbf{U}_n + \Delta t \sum_{j=0}^s \alpha_{sj} \dot{\mathbf{U}}_{n+\gamma_j} \quad (3b)$$

$$\dot{\mathbf{U}}_{n+1} = \dot{\mathbf{U}}_n + \Delta t \sum_{j=0}^s \alpha_{sj} \ddot{\mathbf{U}}_{n+\gamma_j}. \quad (3c)$$

In the initial time  $t_0$ , the initial acceleration vector  $\ddot{\mathbf{U}}_0$  is given by solving the equilibrium equation at  $t_0$  with given initial conditions  $\mathbf{U}_0$  and  $\dot{\mathbf{U}}_0$ .

$$\ddot{\mathbf{U}}_0 = \mathbf{M}^{-1} \{ \mathbf{F}(t_0) - \mathbf{K}\mathbf{U}_0 - \mathbf{C}\dot{\mathbf{U}}_0 \} \quad (4)$$

Hence, the proposed composite  $s$ -sub-step implicit algorithm (2) is obviously self-starting, like the known WBZ- $\alpha$  [8], HHT- $\alpha$  [7], and generalized- $\alpha$  [9, 10] algorithms.

Before the novel implicit method (2) is optimized to determine unknown algorithmic parameters, it is necessary to demonstrate differences between the present method (2) and the authors' previous work [35]. A directly self-starting  $s$ -sub-step implicit method was constructed and developed in [35] to achieve unconditional stability,  $s$ th-order accuracy, no overshoots, and controllable algorithmic dissipation in the high-frequency range. The published directly self-starting  $s$ -sub-step method [35] is written in the  $i$ th sub-step  $t \in [t_n + \gamma_{i-1}\Delta t, t_n + \gamma_i\Delta t]$  as

$$\mathbf{M}\tilde{\mathbf{U}}_{n+\gamma_i} + \mathbf{C}\tilde{\mathbf{U}}_{n+\gamma_i} + \mathbf{K}\tilde{\mathbf{U}}_{n+\gamma_i} = \mathbf{F}(t_n + \gamma_i\Delta t) \quad (5a)$$

$$\tilde{\mathbf{U}}_{n+\gamma_i} = \mathbf{U}_n + \Delta t \sum_{j=1}^i \alpha_{ij} \tilde{\mathbf{U}}_{n+\gamma_j} \quad (5b)$$

$$\tilde{\mathbf{U}}_{n+\gamma_i} = \dot{\mathbf{U}}_n + \Delta t \sum_{j=1}^i \alpha_{ij} \tilde{\mathbf{U}}_{n+\gamma_j} \quad (5c)$$

with the displacement and velocity updates

$$\mathbf{U}_{n+1} = \mathbf{U}_n + \Delta t \sum_{i=1}^s \beta_i \tilde{\mathbf{U}}_{n+\gamma_i} \quad (5d)$$

$$\dot{\mathbf{U}}_{n+1} = \dot{\mathbf{U}}_n + \Delta t \sum_{i=1}^s \beta_i \tilde{\mathbf{U}}_{n+\gamma_i}. \quad (5e)$$

It can be found that the present method (2) differs apparently from the previous method (5) at the algorithm level. In addition, there are other differences between them.

- (a) The previous method (5) is directly self-starting since the acceleration vector  $\ddot{\mathbf{U}}_n$  does not participate in calculating the displacement and velocity updates, whereas the present method (2) is only described to be self-starting since it involves the acceleration vector  $\ddot{\mathbf{U}}_n$ .
- (b) For the previous method (5), numerical solutions at  $t_{n+1}$  do not generally satisfy the second-order equations of motion (1), whereas numerical solutions of the present method (2) exactly satisfy the system (1) at the instant  $t_{n+1}$ .
- (c) Although both of the methods are required to achieve  $s$ th-order accuracy for the output responses ( $\mathbf{U}_{n+1}$ ,  $\dot{\mathbf{U}}_{n+1}$ , and  $\ddot{\mathbf{U}}_{n+1}$ ), the previous method (5) only requires second-order consistency in each sub-step whereas the present method (2) enhances third-order consistency in each sub-step; see Eq. (22).
- (d) In terms of the acceleration accuracy, the previous method (5) requires an additional procedure to achieve the same acceleration accuracy as those in displacement and velocity (see Section 4 of the original study [35]), whereas the present method (2) automatically provides identical order of accuracy in displacement, velocity, and acceleration.

Therefore, the present method (2) is a completely new construction and development using the composite sub-step technique.

## 2.2. Accuracy analysis

It is cumbersome and difficult to analyze numerical properties of an integration algorithm by directly manipulating the multi-degree-of-freedom system (1). However, the modal decomposition technique [1] can be employed to uncouple the system (1) by using the orthogonality properties of the free-vibration mode shapes of the undamped system. As a result, the modal damping is often used. It is therefore convenient to analyze numerical properties of an integration method by solving the standard SDOF system [4, 47, 48], which is written as

$$\ddot{u}(t) + 2\xi\omega\dot{u}(t) + \omega^2 u(t) = f(t) \quad (6)$$

where  $\xi$ ,  $\omega$ , and  $f(t)$  are the damping ratio, the undamped natural frequency of the system, and the modal force, respectively.

For the subsequent use, considering the above SDOF system with given initial displacement  $u_n$  and velocity  $\dot{u}_n$  and external load  $f(t) = \exp(t)$ , its exact displacement and velocity are analytically obtained as

$$\begin{aligned} u(t) &= \exp(-\xi\omega\tau)(\cos(\omega_d\tau) + \frac{\xi\omega}{\omega_d} \sin(\omega_d\tau))u_n + \frac{1}{\omega_d} \exp(-\xi\omega\tau) \sin(\omega_d\tau) \dot{u}_n + \frac{\exp(\tau)}{(\omega^2 + 2\xi\omega + 1)} \\ &\quad - \exp(-\xi\omega\tau) \frac{\omega_d \cos(\omega_d\tau) + (1 + \xi\omega) \sin(\omega_d\tau)}{\omega_d(\omega^2 + 2\xi\omega + 1)} \end{aligned} \quad (7a)$$

$$\begin{aligned} \dot{u}(t) &= -\frac{\omega^2}{\omega_d} \exp(-\xi\omega\tau) \sin(\omega_d\tau) u_n + \frac{1}{\omega_d} \exp(-\xi\omega\tau) (-\xi\omega \sin(\omega_d\tau) + \omega_d \cos(\omega_d\tau)) \dot{u}_n + \frac{\exp(\tau)}{(\omega^2 + 2\xi\omega + 1)} \\ &\quad + \exp(-\xi\omega\tau) \frac{(\omega^2 + \xi\omega) \sin(\omega_d\tau) - \omega_d \cos(\omega_d\tau)}{\omega_d(\omega^2 + 2\xi\omega + 1)} \end{aligned} \quad (7b)$$

where  $\tau = t - t_n$  and  $\omega_d = \sqrt{1 - \xi^2} \cdot \omega$ . Then, the exact solutions at time  $t_{n+1}$  can be collected as

$$\begin{bmatrix} u(t_{n+1}) \\ \dot{u}(t_{n+1}) \end{bmatrix} = \mathbf{D}_{exa} \begin{bmatrix} u_n \\ \dot{u}_n \end{bmatrix} + \mathbf{L}_{exa} \quad (8)$$

where  $\mathbf{D}_{exa}$  is the exact amplification matrix [35, 49], which is

$$\mathbf{D}_{exa} = \exp(-\xi\omega\Delta t) \begin{bmatrix} \cos(\omega_d\Delta t) + \frac{\xi\omega}{\omega_d} \sin(\omega_d\Delta t) & \frac{1}{\omega_d} \sin(\omega_d\Delta t) \\ -\frac{\omega^2}{\omega_d} \sin(\omega_d\Delta t) & -\frac{\xi\omega}{\omega_d} \sin(\omega_d\Delta t) + \cos(\omega_d\Delta t) \end{bmatrix}, \quad (9a)$$

and  $\mathbf{L}_{exa}$  is the exact load operator associated with the external load  $\exp(t)$ .

$$\mathbf{L}_{exa} = \begin{bmatrix} \frac{\exp(\Delta t)}{(\omega^2 + 2\xi\omega + 1)} - \exp(-\xi\omega\Delta t) \frac{\omega_d \cos(\omega_d\Delta t) + (1 + \xi\omega) \sin(\omega_d\Delta t)}{\omega_d(\omega^2 + 2\xi\omega + 1)} \\ \frac{\exp(\Delta t)}{(\omega^2 + 2\xi\omega + 1)} + \exp(-\xi\omega\Delta t) \frac{(\omega^2 + \xi\omega) \sin(\omega_d\Delta t) - \omega_d \cos(\omega_d\Delta t)}{\omega_d(\omega^2 + 2\xi\omega + 1)} \end{bmatrix} \quad (9b)$$

On the other hand, applying the proposed implicit algorithm (2) to solve the SDOF system (6) can yield

$$\ddot{u}_{n+\gamma_i} + 2\xi\omega\dot{u}_{n+\gamma_i} + \omega^2 u_{n+\gamma_i} = f(t_n + \gamma_i \Delta t) \quad (10a)$$

$$u_{n+\gamma_i} = u_n + \Delta t \sum_{j=0}^i \alpha_{ij} \dot{u}_{n+\gamma_j} \quad (10b)$$

$$\dot{u}_{n+\gamma_i} = \dot{u}_n + \Delta t \sum_{j=0}^i \alpha_{ij} \ddot{u}_{n+\gamma_j} \quad (10c)$$

with varying the index  $i \in 1, 2, \dots, s$ . Inserting Eq. (10b) into (10a) to eliminate  $u_{n+\gamma_i}$  gives

$$f(t_n + \gamma_i \Delta t) = \ddot{u}_{n+\gamma_i} + 2\xi\omega\dot{u}_{n+\gamma_i} + \omega^2 \left( u_n + \Delta t \sum_{j=0}^i \alpha_{ij} \dot{u}_{n+\gamma_j} \right) = \left( 2\xi\omega\dot{u}_{n+\gamma_i} + \omega^2 \Delta t \sum_{j=0}^i \alpha_{ij} \dot{u}_{n+\gamma_j} \right) + \ddot{u}_{n+\gamma_i} + \omega^2 u_n. \quad (11)$$

Define the notations  $\dot{\mathbf{Y}}$  and  $\ddot{\mathbf{Y}}$  as  $\dot{\mathbf{Y}} = [\dot{u}_{n+\gamma_0} \quad \dot{u}_{n+\gamma_1} \quad \dots \quad \dot{u}_{n+\gamma_s}]^T$  and  $\ddot{\mathbf{Y}} = [\ddot{u}_{n+\gamma_0} \quad \ddot{u}_{n+\gamma_1} \quad \dots \quad \ddot{u}_{n+\gamma_s}]^T$  and also define  $\mathbf{f}$  as  $\mathbf{f} = [f(t_n + \gamma_0 \Delta t) \quad f(t_n + \gamma_1 \Delta t) \quad \dots \quad f(t_n + \gamma_s \Delta t)]^T$ .

Then, equation (11) with varying  $i = 0, 1, \dots, s$  can be written as

$$(2\xi\omega\mathbf{I} + \omega^2\Delta t\mathbf{A})\dot{\mathbf{Y}} + \ddot{\mathbf{Y}} = \mathbf{f} - \omega^2 u_n \mathbf{1} \quad (12)$$

where  $\mathbf{A}$  is a lower-triangle matrix of dimension  $s+1$  collecting the element  $\alpha_{ij}, i \geq j$ ;  $\mathbf{1}$  is the column vector whose all elements are unity, and  $\mathbf{I}$  is the unity matrix with dimension  $s+1$ . Similarly, equation (10c) can be rewritten as

$$\dot{\mathbf{Y}} - \Delta t\mathbf{A}\ddot{\mathbf{Y}} = \dot{u}_n \mathbf{1}. \quad (13)$$

Solving Eqs. (12) and (13) yields

$$\begin{bmatrix} \dot{\mathbf{Y}} \\ \ddot{\mathbf{Y}} \end{bmatrix} = \begin{bmatrix} 2\xi\omega\mathbf{I} + \omega^2\Delta t\mathbf{A} & \mathbf{I} \\ \mathbf{I} & -\Delta t\mathbf{A} \end{bmatrix}^{-1} \left\{ \begin{bmatrix} \mathbf{f} \\ \mathbf{0} \end{bmatrix} + \begin{bmatrix} -\omega^2\mathbf{1} & \mathbf{0} \\ \mathbf{0} & \mathbf{1} \end{bmatrix} \begin{bmatrix} u_n \\ \dot{u}_n \end{bmatrix} \right\}. \quad (14)$$

where  $\mathbf{0}$  denotes a column vector whose all elements are zero.

Finally, numerical displacement  $u_{n+1}$  and velocity  $\dot{u}_{n+1}$  are updated in the final sub-step due to  $\gamma_s = 1$ , that is Eqs. (3b-c).

$$u_{n+1} = u_n + \Delta t \sum_{j=0}^s \alpha_{sj} \dot{u}_{n+\gamma_j} \quad (15a)$$

$$\dot{u}_{n+1} = \dot{u}_n + \Delta t \sum_{j=0}^s \alpha_{sj} \ddot{u}_{n+\gamma_j} \quad (15b)$$

The above equations can be further written as

$$\begin{bmatrix} u_{n+1} \\ \dot{u}_{n+1} \end{bmatrix} = \begin{bmatrix} 1 & 0 \\ 0 & 1 \end{bmatrix} \begin{bmatrix} u_n \\ \dot{u}_n \end{bmatrix} + \begin{bmatrix} \Delta t\mathbf{b}^T & \mathbf{0}^T \\ \mathbf{0}^T & \Delta t\mathbf{b}^T \end{bmatrix} \begin{bmatrix} \dot{\mathbf{Y}} \\ \ddot{\mathbf{Y}} \end{bmatrix} \quad (16)$$

where the vector  $\mathbf{b}$  is defined as  $\mathbf{b}^T = [\alpha_{s0} \quad \alpha_{s1} \quad \dots \quad \alpha_{ss}]$ . Substituting Eq. (14) into (16) yields

$$\begin{bmatrix} u_{n+1} \\ \dot{u}_{n+1} \end{bmatrix} = \mathbf{D}_{num} \begin{bmatrix} u_n \\ \dot{u}_n \end{bmatrix} + \mathbf{L}_{num} \quad (17)$$

where  $\mathbf{D}_{num}$  and  $\mathbf{L}_{num}$  are called the numerical amplification matrix and the numerical load operator, respectively.

$$\mathbf{D}_{num} = \begin{bmatrix} 1 & 0 \\ 0 & 1 \end{bmatrix} + \begin{bmatrix} \Delta t\mathbf{b}^T & \mathbf{0}^T \\ \mathbf{0}^T & \Delta t\mathbf{b}^T \end{bmatrix} \begin{bmatrix} 2\xi\omega\mathbf{I} + \omega^2\Delta t\mathbf{A} & \mathbf{I} \\ \mathbf{I} & -\Delta t\mathbf{A} \end{bmatrix}^{-1} \begin{bmatrix} -\omega^2\mathbf{1} & \mathbf{0} \\ \mathbf{0} & \mathbf{1} \end{bmatrix} \quad (18a)$$

$$\mathbf{L}_{num} = \begin{bmatrix} \Delta t\mathbf{b}^T & \mathbf{0}^T \\ \mathbf{0}^T & \Delta t\mathbf{b}^T \end{bmatrix} \begin{bmatrix} 2\xi\omega\mathbf{I} + \omega^2\Delta t\mathbf{A} & \mathbf{I} \\ \mathbf{I} & -\Delta t\mathbf{A} \end{bmatrix}^{-1} \begin{bmatrix} \mathbf{f} \\ \mathbf{0} \end{bmatrix} \quad (18b)$$

With the exact and numerical iterative relationships in hand, the conditions achieving  $p$ th-order accuracy for composite  $s$ -sub-step algorithm (2) can be defined as follows.

**Proposition 1.** The composite  $s$ -sub-step algorithm (2) achieves  $p$ th-order accuracy if and only if both  $u_{n+1} - u(t_{n+1}) = O(\Delta t^{p+1})$  and  $\dot{u}_{n+1} - \dot{u}(t_{n+1}) = O(\Delta t^{p+1})$  are satisfied, namely

$$\mathbf{D}_{num} - \mathbf{D}_{exa} = O(\Delta t^{p+1}) \quad (19a)$$

$$\mathbf{L}_{num} - \mathbf{L}_{exa} = O(\Delta t^{p+1}). \quad (19b)$$

Notice that proposition 1 actually requires the numerical scheme in the final sub-step to be  $p$ th-order accurate due to  $\gamma_s = 1$ . To eliminate the redundant algorithmic parameters, an additional requirement is imposed in this paper. In the  $i$ th sub-step  $t \in [t_n + \gamma_{i-1}\Delta t, t_n + \gamma_i\Delta t]$ , the displacement predicted by Eq. (10b) is defined as being  $q$ th-order consistency if  $u(t_n + \gamma_i\Delta t) - u_{n+\gamma_i} = O(\Delta t^q)$  is fulfilled, namely,

$$u(t_n + \gamma_i\Delta t) - \left[ u(t_n) + \Delta t \sum_{j=0}^i \alpha_{ij} \dot{u}(t_n + \gamma_j\Delta t) \right] = O(\Delta t^q). \quad (20)$$

Substituting the Taylor series expansions of  $u(t_n + \gamma_i\Delta t)$  and  $\dot{u}(t_n + \gamma_j\Delta t)$  at time  $t_n$  into the above and then simplifying the result yield

$$u(t_n + \gamma_i\Delta t) - u_{n+\gamma_i} = \left( \gamma_i - \sum_{j=0}^i \alpha_{ij} \right) \Delta t \dot{u}(t_n) + \left( \frac{\gamma_i^2}{2} - \sum_{j=0}^i \alpha_{ij} \gamma_j \right) \Delta t^2 \ddot{u}(t_n) + O(\Delta t^3). \quad (21)$$

Then, the following conditions are satisfied to eliminate low-order terms, reaching a third-order consistency [21].

$$\boxed{\sum_{j=0}^i \alpha_{ij} = \gamma_i \quad \text{and} \quad \sum_{j=0}^i \alpha_{ij} \gamma_j = \frac{\gamma_i^2}{2}, \forall i \in 1, \dots, s} \quad (22)$$

In the case of  $i = 1$ , namely in the first sub-step, the following relations hold.

$$\alpha_{10} + \alpha_{11} = \gamma_1 \quad \alpha_{10}\gamma_0 + \alpha_{11}\gamma_1 = \frac{\gamma_1^2}{2} \quad (23)$$

Due to  $\gamma_0 = 0$ , the above equations give  $\alpha_{10} = \alpha_{11} = \gamma_1/2$ , implying the non-dissipative trapezoidal rule [1] used in the first sub-step  $t \in [t_n, t_n + \gamma_1\Delta t]$ . Note that conditions (22) also ensure a third-order consistency in velocity (10c). As stated previously, the published directly self-starting implicit algorithms [35] only require a second-order consistency in each sub-step.

### 2.3. Dissipation control

The previous section has derived the numerical amplification matrix  $\mathbf{D}_{num}$ , thus it is very easy to design controllable numerical dissipation in the high-frequency range. Firstly, the characteristic polynomial of  $\mathbf{D}_{num}$  is computed as

$$\det(\mathbf{I}_2 - \zeta \mathbf{D}_{num}) = \zeta^2 - 2A_1\zeta + A_2 = 0 \quad (24)$$

where  $\mathbf{I}_2$  denotes the unity matrix with dimension 2, and coefficients  $A_1$  and  $A_2$  are two principal invariants of  $\mathbf{D}_{num}$ . When considering the high-frequency limit  $\omega \rightarrow \infty$ , the characteristic polynomial (24) can be expressed as

$$\zeta_\infty^2 - 2A_{1\infty}\zeta_\infty + A_{2\infty} = 0 \quad (25)$$

where  $A_{1\infty} = \lim_{\omega \rightarrow \infty} A_1$  and  $A_{2\infty} = \lim_{\omega \rightarrow \infty} A_2$ .

On the other hand, the optimal high-frequency dissipation [10, 50] is achieved if and only if eigenvalues of the amplification matrix  $\mathbf{D}_{num}$  become the same real roots, denoted by  $\rho_\infty$ , in the high-frequency limit. Then,

$$(\zeta_\infty - \rho_\infty)^2 = \zeta_\infty^2 - 2\rho_\infty\zeta_\infty + \rho_\infty^2 = 0. \quad (26)$$

Comparing Eqs. (25) and (26) yields the conditions to achieve dissipation control in the high-frequency range.

$$\boxed{A_{1\infty} = \rho_\infty \quad \text{and} \quad A_{2\infty} = \rho_\infty^2} \quad (27)$$

It is necessary to point out that two invariants  $A_1$  and  $A_2$  given by Eq. (24) are often employed to analyze the stability of an integrator. When the following conditions [1] are fulfilled, the proposed algorithms are unconditionally stable.

$$|2A_1| \leq A_2 + 1, \quad -1 \leq A_2 < 1 \quad (28a)$$

$$|A_1| < 1, \quad A_2 = 1 \quad (28b)$$

After embedding high-order accuracy and controllable numerical dissipation in the high-frequency range, the developed implicit algorithm (2) will achieve unconditional stability via selecting proper  $\gamma_1$ . In Section 4, these numerical properties will be validated well.

### 3. High-order accurate schemes

Via the conditions derived in the previous section, the composite  $s$ -sub-step implicit algorithm (2) will be analyzed to achieve controllable numerical dissipation, high-order accuracy, and unconditional stability. As a result, the composite  $s$ -sub-step algorithm (2) with  $s \leq 6$  can generally achieve  $s$ th-order accuracy when simultaneously embedding controllable high-frequency dissipation and unconditional stability. Besides, identical effective stiffness matrices are required for the present implicit method (2) to attain optimal spectral properties [16, 51], which requires

$$\boxed{\alpha_{11} = \alpha_{22} = \cdots = \alpha_{ss}}. \quad (29)$$

The integration algorithms developed in this section are named as SUCIn, where the first four letters denote the sub-step, unconditional stability, controllable numerical dissipation, and identical effective stiffness matrices, while the final letter  $n$  represents either the order of accuracy or the number of sub-steps (*these two quantities are the same in this paper*).

Obviously, the composite  $s$ -sub-step method (2) simply corresponds to the non-dissipative trapezoidal rule in the case of  $s = 1$ . For the two-sub-step case ( $s = 2$ ), the resulting scheme covers the published two-sub-step implicit algorithm [18], also named as SUCI2 in this paper, which is rewritten herein for completeness.

$$\mathbf{M}\ddot{\mathbf{U}}_{n+\gamma_1} + \mathbf{C}\dot{\mathbf{U}}_{n+\gamma_1} + \mathbf{K}\mathbf{U}_{n+\gamma_1} = \mathbf{F}(t_n + \gamma_1\Delta t) \quad \mathbf{M}\ddot{\mathbf{U}}_{n+1} + \mathbf{C}\dot{\mathbf{U}}_{n+1} + \mathbf{K}\mathbf{U}_{n+1} = \mathbf{F}(t_{n+1}) \quad (30a)$$

$$\mathbf{U}_{n+\gamma_1} = \mathbf{U}_n + \Delta t \left( \frac{\gamma_1}{2} \dot{\mathbf{U}}_n + \frac{\gamma_1}{2} \dot{\mathbf{U}}_{n+\gamma_1} \right) \quad \mathbf{U}_{n+1} = \mathbf{U}_n + \Delta t \left( \frac{-\gamma_1^2 + 3\gamma_1 - 1}{2\gamma_1} \dot{\mathbf{U}}_n + \frac{1 - \gamma_1}{2\gamma_1} \dot{\mathbf{U}}_{n+\gamma_1} + \frac{\gamma_1}{2} \dot{\mathbf{U}}_{n+1} \right) \quad (30b)$$

$$\dot{\mathbf{U}}_{n+\gamma_1} = \dot{\mathbf{U}}_n + \Delta t \left( \frac{\gamma_1}{2} \ddot{\mathbf{U}}_n + \frac{\gamma_1}{2} \ddot{\mathbf{U}}_{n+\gamma_1} \right) \quad \dot{\mathbf{U}}_{n+1} = \dot{\mathbf{U}}_n + \Delta t \left( \frac{-\gamma_1^2 + 3\gamma_1 - 1}{2\gamma_1} \ddot{\mathbf{U}}_n + \frac{1 - \gamma_1}{2\gamma_1} \ddot{\mathbf{U}}_{n+\gamma_1} + \frac{\gamma_1}{2} \ddot{\mathbf{U}}_{n+1} \right) \quad (30c)$$

The parameter  $\gamma_1$  controls numerical dissipation in the high-frequency range.

$$\gamma_1 = \frac{2 - \sqrt{2(1 + \rho_\infty)}}{1 - \rho_\infty} \quad (31)$$

where  $\rho_\infty \in [-1, 1]$ . In the case of  $\rho_\infty = 1$ , the parameter  $\gamma_1$  given above should be set as  $1/2$ , covering the composite equal sub-step trapezoidal rule [14].

SUCI2 is optimal with respect to spectral properties since some existing two-sub-step methods, such as the  $\rho_\infty$ -Bathe [15] algorithm, correspond to it when embedding identical effective stiffness matrices within two sub-steps. When achieving a full range of controllable numerical dissipation, only second-order accuracy is obtained for SUCI2.

For the composite  $s$ -sub-step scheme (2), more sub-steps are generally necessary to achieve higher-order accuracy, dissipation control, and unconditional stability. The composite  $s$ -sub-step schemes with  $2 \leq s \leq 6$  will be developed in the following. It should be pointed out that the sub-step splitting ratios  $\gamma_i$  ( $i = 2, \dots, s-1$ ) are not pre-assumed to satisfy the relations  $\gamma_i = i \cdot \gamma_1$ , so the derivations below are general so that the expressions of  $a_{ij}$  are a little complicated for the five- and six-sub-step implicit members.

### 3.1. Three-sub-step third-order scheme: SUCIS

For the three-sub-step scheme, the detailed analysis will be carried out to clearly demonstrate how to determine the unknown algorithmic parameters  $\alpha_{ij}$ . The composite  $s$ -sub-step scheme (2) in the case of  $s = 3$  can be rewritten as follows.

The trapezoidal rule [1] has to be used in the first sub-step  $t \in [t_n, t_n + \gamma_1 \Delta t]$  due to the conditions (22), which is

$$\mathbf{M}\ddot{\mathbf{U}}_{n+\gamma_1} + \mathbf{C}\dot{\mathbf{U}}_{n+\gamma_1} + \mathbf{K}\mathbf{U}_{n+\gamma_1} = \mathbf{F}(t_n + \gamma_1 \Delta t) \quad (32a)$$

$$\mathbf{U}_{n+\gamma_1} = \mathbf{U}_n + \Delta t \left( \frac{\gamma_1}{2} \dot{\mathbf{U}}_n + \frac{\gamma_1}{2} \dot{\mathbf{U}}_{n+\gamma_1} \right) \quad (32b)$$

$$\dot{\mathbf{U}}_{n+\gamma_1} = \dot{\mathbf{U}}_n + \Delta t \left( \frac{\gamma_1}{2} \ddot{\mathbf{U}}_n + \frac{\gamma_1}{2} \ddot{\mathbf{U}}_{n+\gamma_1} \right). \quad (32c)$$

An integration scheme in the second sub-step  $t \in [t_n + \gamma_1 \Delta t, t_n + \gamma_2 \Delta t]$  is given as

$$\mathbf{M}\ddot{\mathbf{U}}_{n+\gamma_2} + \mathbf{C}\dot{\mathbf{U}}_{n+\gamma_2} + \mathbf{K}\mathbf{U}_{n+\gamma_2} = \mathbf{F}(t_n + \gamma_2 \Delta t) \quad (32d)$$

$$\mathbf{U}_{n+\gamma_2} = \mathbf{U}_n + \Delta t \left( \alpha_{20} \dot{\mathbf{U}}_n + \alpha_{21} \dot{\mathbf{U}}_{n+\gamma_1} + \frac{\gamma_1}{2} \dot{\mathbf{U}}_{n+\gamma_2} \right) \quad (32e)$$

$$\dot{\mathbf{U}}_{n+\gamma_2} = \dot{\mathbf{U}}_n + \Delta t \left( \alpha_{20} \ddot{\mathbf{U}}_n + \alpha_{21} \ddot{\mathbf{U}}_{n+\gamma_1} + \frac{\gamma_1}{2} \ddot{\mathbf{U}}_{n+\gamma_2} \right) \quad (32f)$$

and numerical displacement, velocity, and acceleration vectors at  $t_{n+1}$  are obtained by solving the numerical scheme in the third (final) sub-step  $t \in [t_n + \gamma_2 \Delta t, t_n + \gamma_3 \Delta t] = [t_n + \gamma_2 \Delta t, t_{n+1}]$ .

$$\mathbf{M}\ddot{\mathbf{U}}_{n+1} + \mathbf{C}\dot{\mathbf{U}}_{n+1} + \mathbf{K}\mathbf{U}_{n+1} = \mathbf{F}(t_{n+1}) \quad (32g)$$

$$\mathbf{U}_{n+1} = \mathbf{U}_n + \Delta t \left( \alpha_{30} \dot{\mathbf{U}}_n + \alpha_{31} \dot{\mathbf{U}}_{n+\gamma_1} + \alpha_{32} \dot{\mathbf{U}}_{n+\gamma_2} + \frac{\gamma_1}{2} \dot{\mathbf{U}}_{n+1} \right) \quad (32h)$$

$$\dot{\mathbf{U}}_{n+1} = \dot{\mathbf{U}}_n + \Delta t \left( \alpha_{30} \ddot{\mathbf{U}}_n + \alpha_{31} \ddot{\mathbf{U}}_{n+\gamma_1} + \alpha_{32} \ddot{\mathbf{U}}_{n+\gamma_2} + \frac{\gamma_1}{2} \ddot{\mathbf{U}}_{n+1} \right) \quad (32i)$$

Notice that the above scheme (32) has used the conditions (29) to achieve identical effective stiffness matrices within three sub-steps, i.e.  $\alpha_{33} = \alpha_{22} = \alpha_{11} = \gamma_1/2$ . In this case, the resulting scheme can save computational costs for solving linear elastic problems since the triangular factorization of the effective stiffness matrix is required once during the whole simulation. More importantly, identical effective stiffness matrices within each sub-step guarantee optimal spectral properties, that is the maximum numerical dissipation but minimum period elongation error.

#### 3.1.1. Third-order accuracy

In what follows, the accuracy analysis is carried out to determine algorithmic parameters  $\alpha_{ij}, 0 \leq j < i \leq 3$ . Firstly, the conditions (22) in the case of  $i = 2, 3$  are explicitly expressed as

$$\alpha_{20} + \alpha_{21} + \frac{\gamma_1}{2} = \gamma_2 \quad \alpha_{30} + \alpha_{31} + \alpha_{32} + \frac{\gamma_1}{2} = \gamma_3 \quad (33a)$$

$$\alpha_{20}\gamma_0 + \alpha_{21}\gamma_1 + \frac{\gamma_1}{2}\gamma_2 = \frac{\gamma_2^2}{2} \quad \alpha_{30}\gamma_0 + \alpha_{31}\gamma_1 + \alpha_{32}\gamma_2 + \frac{\gamma_1}{2}\gamma_3 = \frac{\gamma_3^2}{2}. \quad (33b)$$

Solving the above conditions with  $\gamma_0 = 0$  and  $\gamma_3 = 1$  gives

$$\alpha_{20} = \frac{-\gamma_1^2 + 3\gamma_1\gamma_2 - \gamma_2^2}{2\gamma_1} \quad \alpha_{21} = \frac{\gamma_2(\gamma_2 - \gamma_1)}{2\gamma_1} \quad \alpha_{30} = \frac{-\gamma_1^2 + (3 - 2\alpha_{32})\gamma_1 + 2\alpha_{32}\gamma_2 - 1}{2\gamma_1} \quad \alpha_{31} = \frac{-2\alpha_{32}\gamma_2 - \gamma_1 + 1}{2\gamma_1}. \quad (34)$$

With the known conditions (34) in hand, the numerical amplification matrix and load operator can be further simplified by using Eq. (18). For the constructed composite three-sub-step algorithm (32),  $\mathbf{A}$ ,  $\mathbf{b}$  and  $\mathbf{f}$  are explicitly given, respectively, as

$$\mathbf{A} = \begin{bmatrix} 0 & 0 & 0 & 0 \\ \frac{\gamma_1}{2} & \frac{\gamma_1}{2} & 0 & 0 \\ \alpha_{20} & \alpha_{21} & \frac{\gamma_1}{2} & 0 \\ \alpha_{30} & \alpha_{31} & \alpha_{32} & \frac{\gamma_1}{2} \end{bmatrix}, \quad \mathbf{b} = \begin{bmatrix} \alpha_{30} \\ \alpha_{31} \\ \alpha_{32} \\ \frac{\gamma_1}{2} \end{bmatrix}, \quad \text{and} \quad \mathbf{f} = \begin{bmatrix} 1 \\ \exp(\gamma_1\Delta t) \\ \exp(\gamma_2\Delta t) \\ \exp(\Delta t) \end{bmatrix}. \quad (35)$$

Using the proposition 1 and conditions (34), numerical errors in the amplification matrix and load operator of SUCI3 are calculated as

$$\mathbf{D}_{num} - \mathbf{D}_{exa} = \begin{bmatrix} -\frac{\xi\omega^3 c_{30}}{6} \Delta t^3 + O(\Delta t^4) & \frac{(1-4\xi^2)\omega^2 c_{30}}{12} \Delta t^3 + O(\Delta t^4) \\ \frac{(4\xi^2-1)\omega^4 c_{30}}{12} \Delta t^3 + O(\Delta t^4) & \frac{\xi(2\xi^2-1)\omega^3 c_{30}}{3} \Delta t^3 + O(\Delta t^4) \end{bmatrix} \quad (36a)$$

$$\mathbf{L}_{num} - \mathbf{L}_{exa} = \begin{bmatrix} \frac{(2\xi\omega-1)c_{30}}{12} \Delta t^3 + O(\Delta t^4) \\ \frac{(2\xi\omega-1+\omega^2(1-4\xi^2))c_{30}}{12} \Delta t^3 + O(\Delta t^4) \end{bmatrix} \quad (36b)$$

where  $c_{30} = 6(\gamma_1 - \gamma_2)\gamma_2\alpha_{32} + 3\gamma_1^2 - 6\gamma_1 + 2$ . Obviously,  $c_{30} = 0$  is solved to achieve third-order accuracy, namely

$$\alpha_{32} = \frac{3\gamma_1^2 - 6\gamma_1 + 2}{6\gamma_2(\gamma_2 - \gamma_1)}. \quad (37)$$

### 3.1.2. Unconditional stability

The unconditional stability of SUCI3 is analyzed herein as a demonstration. After achieving third-order accuracy, the characteristic polynomial (24) in the case of  $s = 3$  can be simplified and its principal invariants ( $A_1$  and  $A_2$ ) are given in the absence of  $\xi$  as

$$A_1 = \frac{\gamma_1^3(3\gamma_1^3 - 18\gamma_1^2 + 18\gamma_1 - 4)\Omega^6 + \gamma_1(36\gamma_1^3 + 24\gamma_1^2 - 144\gamma_1 + 48)\Omega^4 + (144\gamma_1^2 - 96)\Omega^2 + 192}{3(\gamma_1^2\Omega^2 + 4)^3} \quad (38a)$$

$$A_2 = \frac{3(3\gamma_1^3 - 18\gamma_1^2 + 18\gamma_1 - 4)\Omega^6 + 12(9\gamma_1^4 + 12\gamma_1^3 - 36\gamma_1^2 + 24\gamma_1 - 4)\Omega^4 + 432\gamma_1^2\Omega^2 + 576}{9(\gamma_1^2\Omega^2 + 4)^3} \quad (38b)$$

where  $\Omega = \omega \cdot \Delta t$ . Due to the quantity  $A_1^2 - A_2 = -576((\gamma_1 - 1)\gamma_1^2(\gamma_1 - 1/3)\Omega^4 + (2\gamma_1^2 - 4/9)\Omega^2 + 8/3)^2 \Omega^2 / (\gamma_1^2\Omega^2 + 4)^6 \leq 0$ , two eigenvalues of the amplification matrix can be expressed as

$$\zeta_{1,2} = A_1 \pm \sqrt{A_2 - A_1^2} \text{Im} \quad (39)$$

where  $\text{Im}$  denotes the imaginary unit being defined as  $\text{Im} = \sqrt{-1}$ . According to the definition [1] of the spectral radius ( $\rho$ ), SUCI3's spectral radius ( $\rho$ ) is simply calculated as

$$\rho = \max(|\zeta_{1,2}|) = \sqrt{A_2}. \quad (40)$$

Note that  $A_2 \geq 0$  is indicated by  $A_1^2 - A_2 \leq 0$ . In this case, the proposed SUCI3 method is said to be unconditionally stable if and only if  $\rho \leq 1$  for all  $\Omega \in [0, \infty)$ .

$$A_2 - 1 = -\frac{24\Omega^4}{(\gamma_1^2\Omega^2 + 4)^6} \cdot \left[ \left(\gamma_1 - \frac{1}{3}\right) \left(\gamma_1 - \frac{2}{3}\right) (\gamma_1^3 - 3\gamma_1^2 + 3\gamma_1 - \frac{2}{3})\Omega^2 - \frac{4}{3}\gamma_1^3 + 4\gamma_1^2 - \frac{8}{3}\gamma_1 + \frac{4}{9} \right] \quad (41)$$

where  $\aleph$  denotes a complicated factor and it is always greater than zero. When the parameter  $\gamma_1$  is determined to control high-frequency dissipation (see Table 1), the quantity  $A_2 - 1$  is always less than zero for all  $\Omega \in [0, \infty)$ , thus validating unconditional stability of SUCI3. Note that  $A_2 - 1$  cannot reach zero for all  $\Omega \in [0, \infty)$  so that SUCI3 with  $\rho_\infty = 1$  ( $\gamma_1 = 2/3$ ) is not completely non-dissipative. As shown later, SUCI3 with  $\rho_\infty = 1$  inevitably imposes some dissipation in the middle-frequency range. This is the case for the published high-order implicit methods [34, 35].

### 3.1.3. Dissipation control

Now, the present three-sub-step scheme (32) leaves  $\gamma_1$  and  $\gamma_2$  to be determined. The controllable numerical dissipation is achieved to determine  $\gamma_1$ . After complicated computations, the characteristic polynomial (25) of the numerical amplification matrix  $\mathbf{D}_{num}$  can be simplified in the high-frequency limit  $\omega \rightarrow \infty$  as

$$\left( \zeta_\infty - \frac{3\gamma_1^3 - 18\gamma_1^2 + 18\gamma_1 - 4}{3\gamma_1^3} \right)^2 = 0. \quad (42)$$

Then, the conditions (27) can give

$$\frac{3\gamma_1^3 - 18\gamma_1^2 + 18\gamma_1 - 4}{3\gamma_1^3} = \rho_\infty. \quad (43)$$

It is difficult to obtain the analytical expression of  $\gamma_1$  in terms of  $\rho_\infty$  by solving Eq. (43), so numerical solutions are solved and given in Table 1. Note that the values of  $\gamma_1$  in Table 1 have carefully chosen to make the corresponding integration schemes unconditionally stable. The parameter  $\gamma_2$  is free except for  $\gamma_2 \neq \gamma_1$  and it has no influence on linear numerical properties. In this paper,  $\gamma_2 = (3 + \sqrt{3})\gamma_1/3$  is used to achieve fourth-order consistency in time  $t_n + \gamma_2\Delta t$ . Of course, the  $\gamma_2 = 2 \cdot \gamma_1$  is also recommended and already used in [21, 34].

It is necessary to stress that the proposed SUCI3 method is more generalized than MSSTH3 [34] since the former does not preinstall  $\gamma_2 = 2 \cdot \gamma_1$  to make the first two sub-steps identical. For example, the  $\gamma_2 = (1 + \gamma_1)/2$  can also be set in SUCI3 to make the last two sub-steps identical.

Table 1: The parameter  $\gamma_1$  of the high-order accurate composite  $s$ -sub-step algorithms for each given  $\rho_\infty \in [0, 1]$ .

$\rho_\infty$	SUCI3	SUCI4	SUCI5	SUCI6
0.0	0.8717330430	1.1456321252	0.5561076823	0.6682847341
0.1	0.8429736308	1.0967332903	0.5482826121	0.6557502542
0.2	0.8170015790	1.0527729141	0.5409197735	0.6440471963
0.3	0.7932944182	1.0126602385	0.5339560879	0.6330349995
0.4	0.7714620009	0.9755949496	0.5273404634	0.6226034838
0.5	0.7512044500	0.9409611552	0.5210308332	0.6126639724
0.6	0.7322856202	0.9082615701	0.5149920597	0.6031433531
0.7	0.7145156239	0.8770723798	0.5091944163	0.5939799400
0.8	0.6977389062	0.8470075321	0.5036124624	0.5851204729
0.9	0.6818258455	0.8176837322	0.4982241931	0.5765178426
1.0	0.6666666666	0.7886751346	0.4930103863	0.5681292760

### 3.2. Four-sub-step fourth-order scheme: SUCI4

Following the same development path as SUCI3, the composite four-sub-step implicit member can be developed to achieve fourth-order accuracy, controllable numerical dissipation, and unconditional stability. However, the de-

tailed analysis is omitted to save the length of this paper, but some important results are given herein.

The composite four-sub-step scheme is explicitly described as follows. The trapezoidal rule [1] given by Eqs. (32a-c) is used in the first sub-step  $t \in [t_n, t_n + \gamma_1 \Delta t]$ , and the numerical scheme in the second sub-step is completely the same as Eqs. (32d-f). In the third sub-step  $t \in [t_n + \gamma_2 \Delta t, t_n + \gamma_3 \Delta t]$ , the numerical scheme is constructed as

$$\mathbf{M}\ddot{\mathbf{U}}_{n+\gamma_3} + \mathbf{C}\dot{\mathbf{U}}_{n+\gamma_3} + \mathbf{K}\mathbf{U}_{n+\gamma_3} = \mathbf{F}(t_n + \gamma_3 \Delta t) \quad (44a)$$

$$\mathbf{U}_{n+\gamma_3} = \mathbf{U}_n + \Delta t \left( \alpha_{30}\dot{\mathbf{U}}_n + \alpha_{31}\dot{\mathbf{U}}_{n+\gamma_1} + \alpha_{32}\dot{\mathbf{U}}_{n+\gamma_2} + \frac{\gamma_1}{2}\dot{\mathbf{U}}_{n+\gamma_3} \right) \quad (44b)$$

$$\dot{\mathbf{U}}_{n+\gamma_3} = \dot{\mathbf{U}}_n + \Delta t \left( \alpha_{30}\ddot{\mathbf{U}}_n + \alpha_{31}\ddot{\mathbf{U}}_{n+\gamma_1} + \alpha_{32}\ddot{\mathbf{U}}_{n+\gamma_2} + \frac{\gamma_1}{2}\ddot{\mathbf{U}}_{n+\gamma_3} \right) \quad (44c)$$

and displacement, velocity, and acceleration vectors at  $t_{n+1}$  are advanced by solving

$$\mathbf{M}\ddot{\mathbf{U}}_{n+1} + \mathbf{C}\dot{\mathbf{U}}_{n+1} + \mathbf{K}\mathbf{U}_{n+1} = \mathbf{F}(t_{n+1}) \quad (44d)$$

$$\mathbf{U}_{n+1} = \mathbf{U}_n + \Delta t \left( \alpha_{40}\dot{\mathbf{U}}_n + \alpha_{41}\dot{\mathbf{U}}_{n+\gamma_1} + \alpha_{42}\dot{\mathbf{U}}_{n+\gamma_2} + \alpha_{43}\dot{\mathbf{U}}_{n+\gamma_3} + \frac{\gamma_1}{2}\dot{\mathbf{U}}_{n+1} \right) \quad (44e)$$

$$\dot{\mathbf{U}}_{n+1} = \dot{\mathbf{U}}_n + \Delta t \left( \alpha_{40}\ddot{\mathbf{U}}_n + \alpha_{41}\ddot{\mathbf{U}}_{n+\gamma_1} + \alpha_{42}\ddot{\mathbf{U}}_{n+\gamma_2} + \alpha_{43}\ddot{\mathbf{U}}_{n+\gamma_3} + \frac{\gamma_1}{2}\ddot{\mathbf{U}}_{n+1} \right). \quad (44f)$$

Obviously, the above scheme has shared identical effective stiffness matrices within each sub-step. There are twelve algorithmic parameters to be determined. The accuracy conditions (22) and (19) can express all  $\alpha_{ij}$  as the functions of  $\gamma_i$ .

$$\alpha_{20} = \frac{-\gamma_1^2 + 3\gamma_1\gamma_2 - \gamma_2^2}{2\gamma_1}$$

$$\alpha_{21} = \frac{\gamma_2(\gamma_2 - \gamma_1)}{2\gamma_1} \quad (45a)$$

$$\alpha_{30} = \frac{-\gamma_1^2 + (3\gamma_3 - 2\alpha_{32})\gamma_1 + 2\alpha_{32}\gamma_2 - \gamma_3^2}{2\gamma_1}$$

$$\alpha_{31} = \frac{-2\alpha_{32}\gamma_2 - \gamma_1\gamma_3 + \gamma_3^2}{2\gamma_1} \quad (45b)$$

$$\alpha_{40} = \frac{-\gamma_1^2 + (3 - 2\alpha_{42} - 2\alpha_{43})\gamma_1 + 2\alpha_{42}\gamma_2 + 2\alpha_{43}\gamma_3 - 1}{2\gamma_1}$$

$$\alpha_{41} = \frac{-2\alpha_{42}\gamma_2 - 2\alpha_{43}\gamma_3 - \gamma_1 + 1}{2\gamma_1} \quad (45c)$$

$$\alpha_{32} = \frac{-3\gamma_1^3 + 9\gamma_1^2 - 6\gamma_1 + 1}{12\alpha_{43}\gamma_2(\gamma_2 - \gamma_1)}$$

$$\alpha_{42} = \frac{6\alpha_{43}\gamma_1\gamma_3 - 6\alpha_{43}\gamma_3^2 + 3\gamma_1^2 - 6\gamma_1 + 2}{6\gamma_2(\gamma_2 - \gamma_1)} \quad (45d)$$

$$\alpha_{43} = \frac{6(1 - \gamma_2)\gamma_1^2 + 12\gamma_1\gamma_2 - 10\gamma_1 - 4\gamma_2 + 3}{12\gamma_3(\gamma_3 - \gamma_2)(\gamma_3 - \gamma_1)} \quad (45e)$$

Like the previous SUCI3 scheme, the fourth-order SUCI4 leaves three splitting ratios of sub-step size, namely  $\gamma_1, \gamma_2$  and  $\gamma_3$ , to be determined. Next, the controllable numerical dissipation in the high-frequency range is imposed to determine  $\gamma_1$ .

In the high-frequency limit  $\omega \rightarrow \infty$ , the resulting characteristic polynomial (25) is further simplified as

$$\left( \zeta_\infty - \frac{3\gamma_1^4 - 24\gamma_1^3 + 36\gamma_1^2 - 16\gamma_1 + 2}{3\gamma_1^4} \right)^2 = 0. \quad (46)$$

Then, the conditions (27) achieving controllable numerical dissipation give

$$\frac{3\gamma_1^4 - 24\gamma_1^3 + 36\gamma_1^2 - 16\gamma_1 + 2}{3\gamma_1^4} = \rho_\infty. \quad (47)$$

Solving the equation above gives values of  $\gamma_1$  for each given  $\rho_\infty \in [0, 1]$ , which are recorded in Table 1. Besides,  $\gamma_2 = 2 \cdot \gamma_1$  and  $\gamma_3 = 3 \cdot \gamma_1$  are used by default in this paper.

### 3.3. Five-sub-step fifth-order scheme: SUCI5

Analogously to the previous SUCI3 and SUCI4 schemes, the composite five-sub-step method is developed by using the theoretical results in Section 2 to achieve fifth-order accuracy, dissipation control, and unconditional stability.

The developed composite five-sub-step algorithm employs the same numerical schemes in the first three sub-steps as SUCI4, which are Eqs. (32a-f) and (44a-c). In the fourth and fifth sub-steps, numerical schemes are explicitly given as

$$\mathbf{M}\ddot{\mathbf{U}}_{n+\gamma_4} + \mathbf{C}\dot{\mathbf{U}}_{n+\gamma_4} + \mathbf{K}\mathbf{U}_{n+\gamma_4} = \mathbf{F}(t_n + \gamma_4 \Delta t) \quad (48a)$$

$$\mathbf{U}_{n+\gamma_4} = \mathbf{U}_n + \Delta t \left( \sum_{j=0}^3 \alpha_{4j} \dot{\mathbf{U}}_{n+\gamma_j} + \frac{\gamma_1}{2} \dot{\mathbf{U}}_{n+\gamma_4} \right) \quad (48b)$$

$$\dot{\mathbf{U}}_{n+\gamma_4} = \dot{\mathbf{U}}_n + \Delta t \left( \sum_{j=0}^3 \alpha_{4j} \ddot{\mathbf{U}}_{n+\gamma_j} + \frac{\gamma_1}{2} \ddot{\mathbf{U}}_{n+\gamma_4} \right). \quad (48c)$$

Again, identical effective stiffness matrices within each sub-step have been achieved by requiring  $\alpha_{ii} = \gamma_1/2$  ( $i = 1, 2, \dots, 5$ ).

There are nineteen algorithmic parameters to be determined. The fifth-order accurate conditions (19), as well as Eq. (22), are used to determine  $\alpha_{ij}$ , which are

$$\alpha_{20} = \frac{-\gamma_1^2 + 3\gamma_1\gamma_2 - \gamma_2^2}{2\gamma_1} \quad \alpha_{21} = \frac{\gamma_2(\gamma_2 - \gamma_1)}{2\gamma_1} \quad (49a)$$

$$\alpha_{30} = \frac{-\gamma_1^2 + (3\gamma_3 - 2\alpha_{32})\gamma_1 + 2\alpha_{32}\gamma_2 - \gamma_3^2}{2\gamma_1} \quad \alpha_{31} = \frac{-2\alpha_{32}\gamma_2 - \gamma_1\gamma_3 + \gamma_3^2}{2\gamma_1} \quad (49b)$$

$$\alpha_{40} = \frac{-\gamma_1^2 + (3\gamma_4 - 2\alpha_{42} - 2\alpha_{43})\gamma_1 + 2\alpha_{42}\gamma_2 + 2\alpha_{43}\gamma_3 - \gamma_4^2}{2\gamma_1} \quad \alpha_{41} = \frac{-2\alpha_{42}\gamma_2 - 2\alpha_{43}\gamma_3 - \gamma_1\gamma_4 + \gamma_4^2}{2\gamma_1} \quad (49c)$$

$$\alpha_{50} = \frac{-\gamma_1^2 + (3 - 2\alpha_{52} - 2\alpha_{53} - 2\alpha_{54})\gamma_1 + 2\alpha_{52}\gamma_2 + 2\alpha_{53}\gamma_3 + 2\alpha_{54}\gamma_4 - 1}{2\gamma_1} \quad (49d)$$

$$\alpha_{51} = \frac{-2\alpha_{52}\gamma_2 - 2\alpha_{53}\gamma_3 - 2\alpha_{54}\gamma_4 - \gamma_1 + 1}{2\gamma_1} \quad \alpha_{32} = \frac{15\gamma_1^4 - 60\gamma_1^3 + 60\gamma_1^2 - 20\gamma_1 + 2}{120\alpha_{43}\alpha_{54}\gamma_2(\gamma_2 - \gamma_1)} \quad (49e)$$

$$\alpha_{42} = \frac{\left\{ \begin{array}{l} 15\alpha_{53}\gamma_1^4 + 30(\alpha_{43}\alpha_{54} - 2\alpha_{53})\gamma_1^3 + 30(2\alpha_{53} - 3\alpha_{43}\alpha_{54})\gamma_1^2 \\ + 20(-6\alpha_{43}^2\alpha_{54}^2\gamma_3 + 3\alpha_{43}\alpha_{54} - \alpha_{53})\gamma_1 + 120\alpha_{43}^2\alpha_{54}^2\gamma_3^2 - 10\alpha_{43}\alpha_{54} + 2\alpha_{53} \end{array} \right\}}{120\alpha_{43}\alpha_{54}^2\gamma_2(\gamma_1 - \gamma_2)} \quad (49f)$$

$$\alpha_{52} = \frac{3\gamma_1^2 + 6(\alpha_{53}\gamma_3 + \alpha_{54}\gamma_4 - 1)\gamma_1 - 6\alpha_{53}\gamma_3^2 - 6\alpha_{54}\gamma_4^2 + 2}{6\gamma_2(\gamma_2 - \gamma_1)} \quad (49g)$$

$$\alpha_{43} = \frac{\gamma_4(\gamma_4 - \gamma_1)(\gamma_4 - \gamma_2)(\gamma_4 - \gamma_3)(15\gamma_1^3\gamma_2 - 15\gamma_1^3 - 45\gamma_1^2\gamma_2 + 35\gamma_1^2 + 30\gamma_1\gamma_2 - 20\gamma_1 - 5\gamma_2 + 3)}{\gamma_3(\gamma_3 - \gamma_1)(\gamma_3 - \gamma_2)G(\gamma_3)} \quad (49h)$$

$$\alpha_{53} = \frac{G(\gamma_4)}{60\gamma_3(\gamma_3 - \gamma_4)(\gamma_2 - \gamma_3)(\gamma_1 - \gamma_3)} \quad \alpha_{54} = \frac{G(\gamma_3)}{60\gamma_4(\gamma_4 - \gamma_3)(\gamma_4 - \gamma_2)(\gamma_4 - \gamma_1)} \quad (49i)$$

where  $G(x) = 30(1-x)(1-\gamma_2)\gamma_1^2 + (50x - 45 + 10(5-6x)\gamma_2)\gamma_1 + 5(4x-3)\gamma_2 - 15x + 12$ .

The resulting scheme leaves  $\gamma_i$  ( $i = 2, 3, 4$ ) as free parameters while  $\gamma_1$  is given to control numerical dissipation in the high-frequency range. In the high-frequency limit  $\omega \rightarrow \infty$ , the characteristic polynomial (25) of SUCI5 is simplified as

$$\left( \zeta_\infty - \frac{15\gamma_1^5 - 150\gamma_1^4 + 300\gamma_1^3 - 200\gamma_1^2 + 50\gamma_1 - 4}{15\gamma_1^5} \right)^2 = 0. \quad (50)$$

The controllable numerical dissipation is achieved by solving

$$\frac{15\gamma_1^5 - 150\gamma_1^4 + 300\gamma_1^3 - 200\gamma_1^2 + 50\gamma_1 - 4}{15\gamma_1^5} = \rho_\infty. \quad (51)$$

For each given  $\rho_\infty$ , the corresponding  $\gamma_1$  is numerically computed and recorded in Table 1. The remaining  $\gamma_2$ ,  $\gamma_3$ , and  $\gamma_4$  can be taken by default as  $\gamma_2 = 2 \cdot \gamma_1$ ,  $\gamma_3 = 3 \cdot \gamma_1$ , and  $\gamma_4 = 4 \cdot \gamma_1$ , respectively, since they have no influence on linear numerical properties.

Following the same development path as the three-, four-, and five-sub-step members, one can propose the six-sub-step member with sixth-order accuracy; see Appendix A for more details. Note that this paper does not pre-assume that the first  $(s-1)$  sub-steps in the general  $s$ -sub-step implicit method (2) share the same length, that is,  $\gamma_j = j \cdot \gamma_1$  ( $j = 2, \dots, s-1$ ), so the developed high-order members are more general and thus the parameters  $a_{ij}$  are a little complicated. As a result, users can make the high-order members possess the same length either in the first  $(s-1)$  sub-steps by forcing  $\gamma_j = j \cdot \gamma_1$  ( $j = 2, \dots, s-1$ ) or in the last  $(s-1)$  sub-steps by forcing  $1 - \gamma_{s-1} = \gamma_{s-1} - \gamma_{s-2} = \dots = \gamma_2 - \gamma_1$ . This paper adopts the former to make the first  $(s-1)$  sub-steps identical.

In summary, this section has developed four novel high-order accurate implicit algorithms. For  $2 \leq s \leq 6$ , the composite  $s$ -sub-step scheme (2) can achieve simultaneously  $s$ th-order accuracy and a full range of dissipation control. However, this case is not true for  $s \geq 7$ . For instance, the composite seven-sub-step implicit scheme within the framework of (2) cannot achieve seventh-order accuracy and controllable numerical dissipation since the resulting scheme is unconditionally unstable. Hence, the high-order accurate algorithms proposed in this paper end up with  $s = 6$ .

#### 4. Spectral properties

In this section, spectral properties of SUCIn will be analyzed and compared. The percentage amplitude decay and relative period error are employed to measure numerical dissipation and dispersion of an integrator, respectively, and their mathematical derivations refer to the literature [1]. In addition, the unconditional stability will be validated by plotting spectral radii in the undamped and damped cases. The published second-order two-sub-step implicit scheme (SUCI2) [18] and the well-known generalized- $\alpha$  method [9, 10] are used herein for reference purposes.

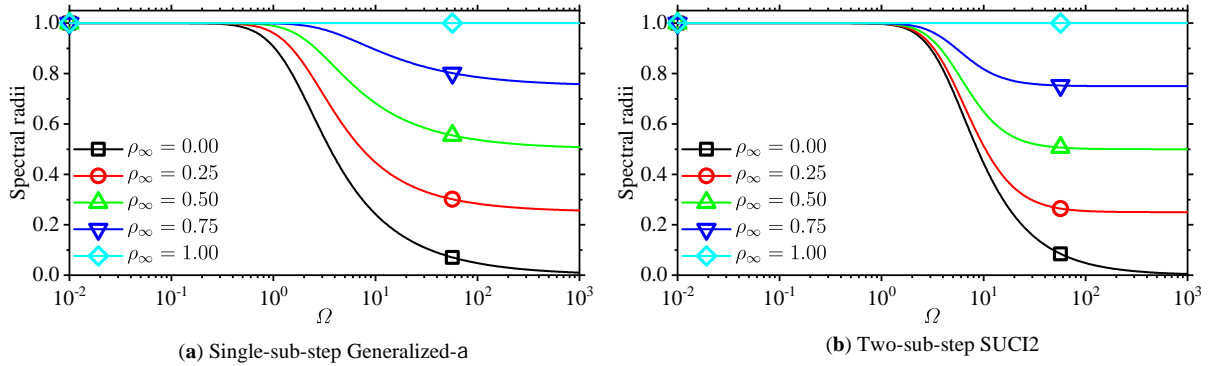
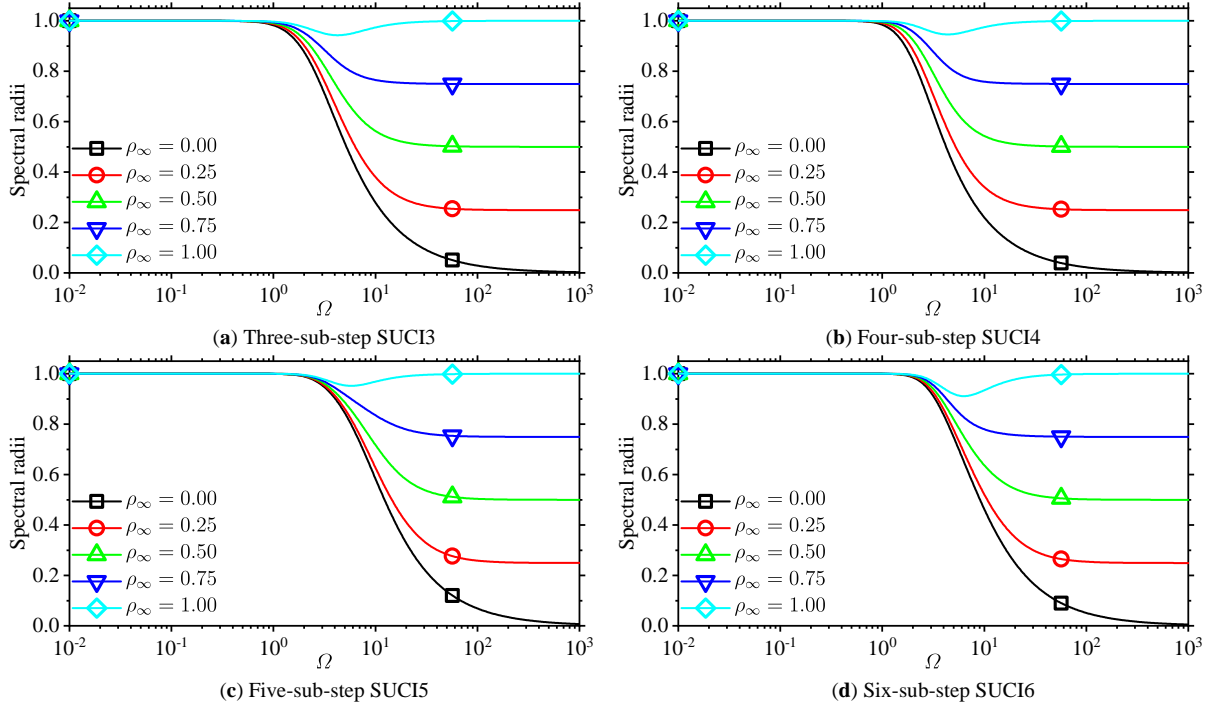


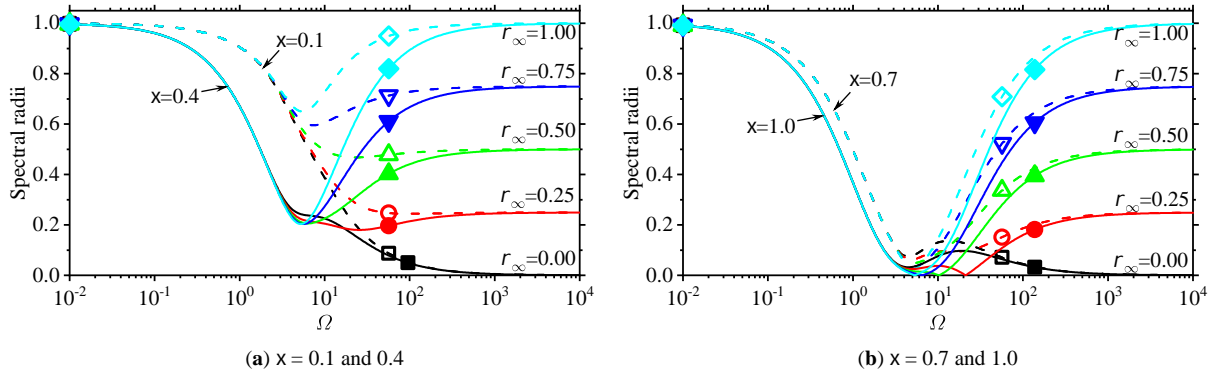
Fig. 1: Spectral radii of the generalized- $\alpha$  [9, 10] and two-sub-step SUCI2 [18] algorithms in the absence of  $\xi$ .

Fig. 1 first plots spectral radii of generalized- $\alpha$  [9, 10] and SUCI2 [18] in the absence  $\xi$ . It can be seen that the parameter  $\rho_\infty$  denoting the spectral radius in the high-frequency limit exactly controls spectral radii in the high-frequency range and the two-sub-step SUCI2 scheme imposes less dissipation in the low-frequency range. Next, spectral radii of four high-order integration algorithms in the case of  $\xi = 0$  are plotted in Fig. 2, where four high-order algorithms achieve controllable spectral radii in the high-frequency range by adjusting  $\rho_\infty$ , thus controlling numerical dissipation. Note that in the non-dissipative case ( $\rho_\infty = 1$ ), four high-order algorithms impose some dissipation in the middle-frequency range (about  $\Omega \in [2, 10]$ ) since their spectral radii are mildly less than unity. This phenomenon has also been observed in [16, 34, 35]. Fig. 2 clearly demonstrates that four novel high-order algorithms achieve unconditional stability in the undamped case. When considering damped cases, four novel high-order algorithms are still



**Fig. 2:** Spectral radii of four novel high-order integration algorithms in the absence of  $\xi$ .

unconditionally stable. To illustrate this fact, taking six-sub-step SUCI6 as an example, Fig. 3 plots spectral radii of SUCI6 in four damped cases. Again, the unconditional stability of SUCI6 is confirmed well. In general, the viscous damping ratio  $\xi$  has an influence on spectral radii in the middle-frequency range, as shown in Fig. 3. With the increase of  $\xi$ , more dissipation is imposed only in the middle-frequency range instead of the high-frequency range.



**Fig. 3:** Spectral radii of six-sub-step SUCI6 when considering four cases of  $\xi$ : (a)  $\xi = 0.1$  and  $0.5$  and (b)  $\xi = 0.7$  and  $1.0$ .

The percentage amplitude decays of various algorithms are plotted in Figs. 4 and 5, where some important observations are found and collected as follows.

- (a) Among the algorithms shown herein, the single-step generalized- $\alpha$  method [9, 10] produces the largest amplitude decays in the low-frequency range while the fifth-order accurate SUCI5 scheme provides the smallest amplitude decays. The previous literature [16] has already reported that the second-order multi-sub-step implicit schemes generally produce fewer amplitude decays in the low-frequency range as the number of sub-step increases. However, this fact is not seemly true for the higher-order sub-step algorithms since the higher-order SUCI3 and SUCI4

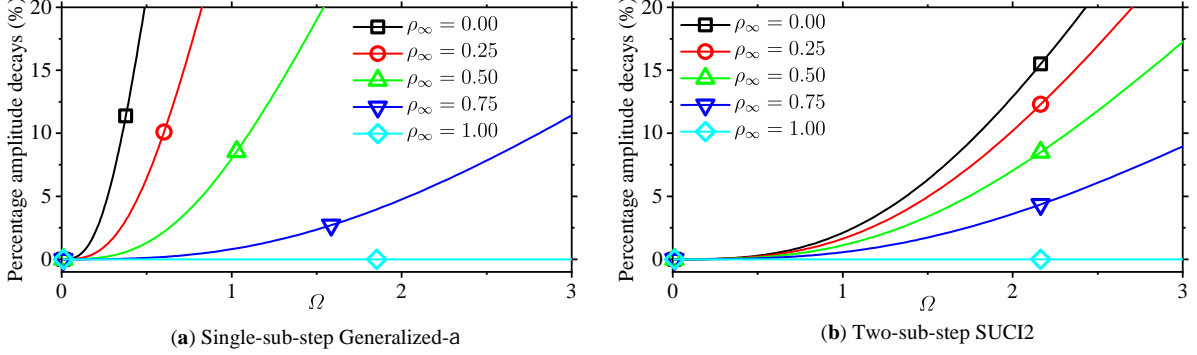


**Fig. 4:** Percentage amplitude decays of the generalized- $\alpha$  [9, 10] and two-sub-step SUCI2 [18] algorithms in the absence of  $\xi$ .

schemes obviously provide larger amplitude decays than second-order SUCI2. In addition, SUCI6 also produces larger amplitude decays than SUCI5.

- (b) Unlike the generalized- $\alpha$  [9, 10] and SUCI2 [18] algorithms, four high-order methods also impose some amplitude decays in the non-dissipative ( $\rho_\infty = 1$ ) case since their spectral radii in the middle-frequency range  $\Omega \in [2, 10]$  are less than unity, as shown in Fig. 2. However, amplitude decays in  $\rho_\infty = 1$  finally decrease to zero with the increase of  $\Omega$ , although they are not shown herein for brevity.
- (c) Amplitude decays of each integration algorithm increase with the decrease of  $\rho_\infty$ , thus controlling numerical dissipation by changing  $\rho_\infty$ .

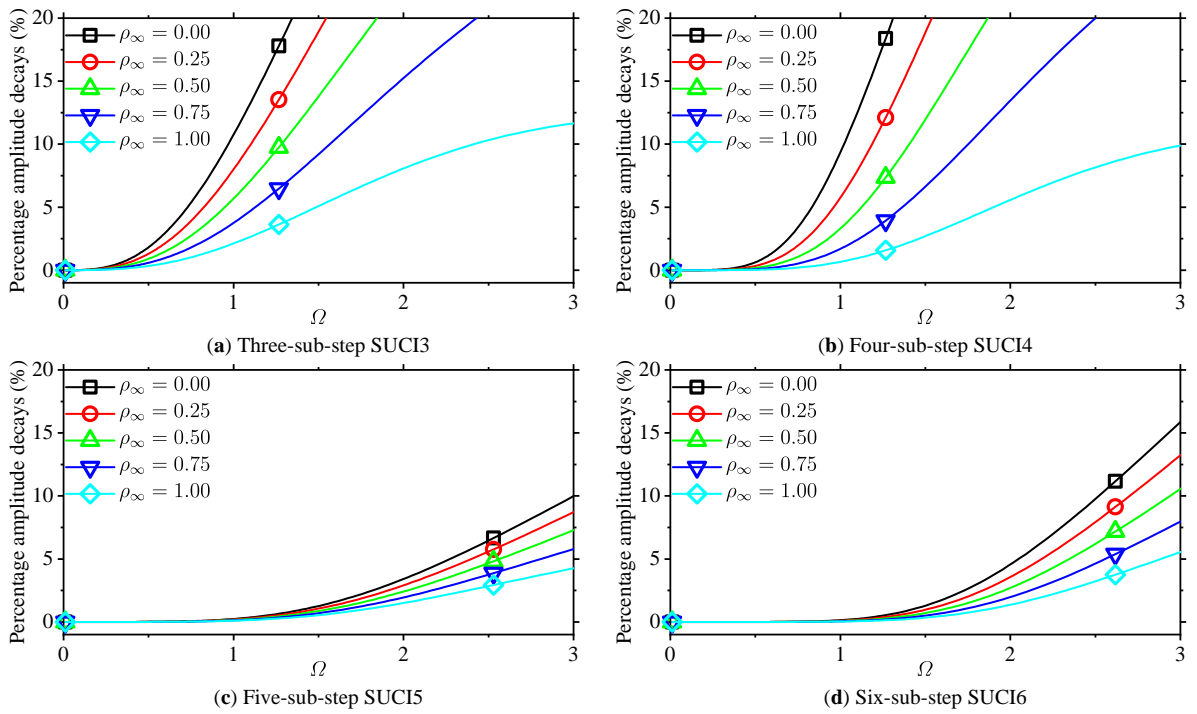


**Fig. 5:** Percentage amplitude decays of four novel high-order integration algorithms in the absence of  $\xi$ .

The period error actually characterizes the precision of an integrator, so a higher-order accurate integration algorithm should produce fewer period errors in the low-frequency range than the lower-order scheme. This fact is

confirmed well for SUCIn. Figs. 6 and 7 show percentage period errors of the generalized- $\alpha$  and SUCIn algorithms. It is pronounced that the higher-order accurate integration algorithm produces fewer period errors and the non-dissipative case provides the smallest period errors for each integration algorithm.

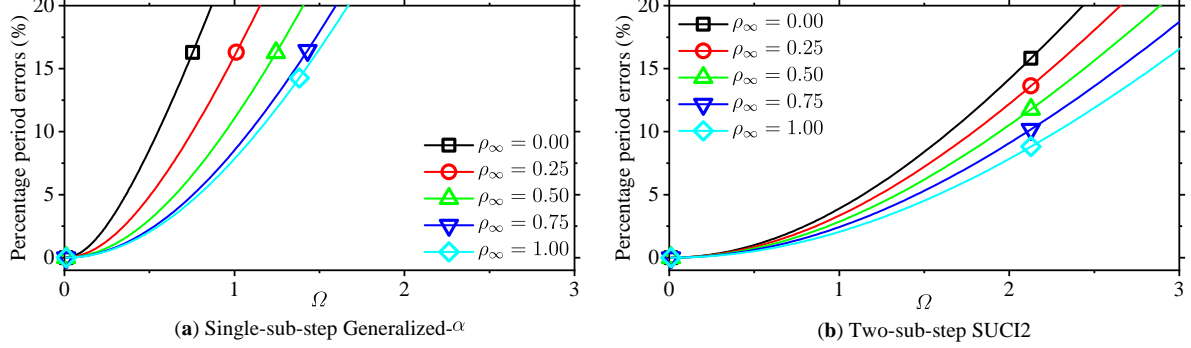


**Fig. 6:** Percentage period errors of the generalized- $\alpha$  [9, 10] and two-sub-step SUCI2 [18] algorithms in the absence of  $\xi$ .

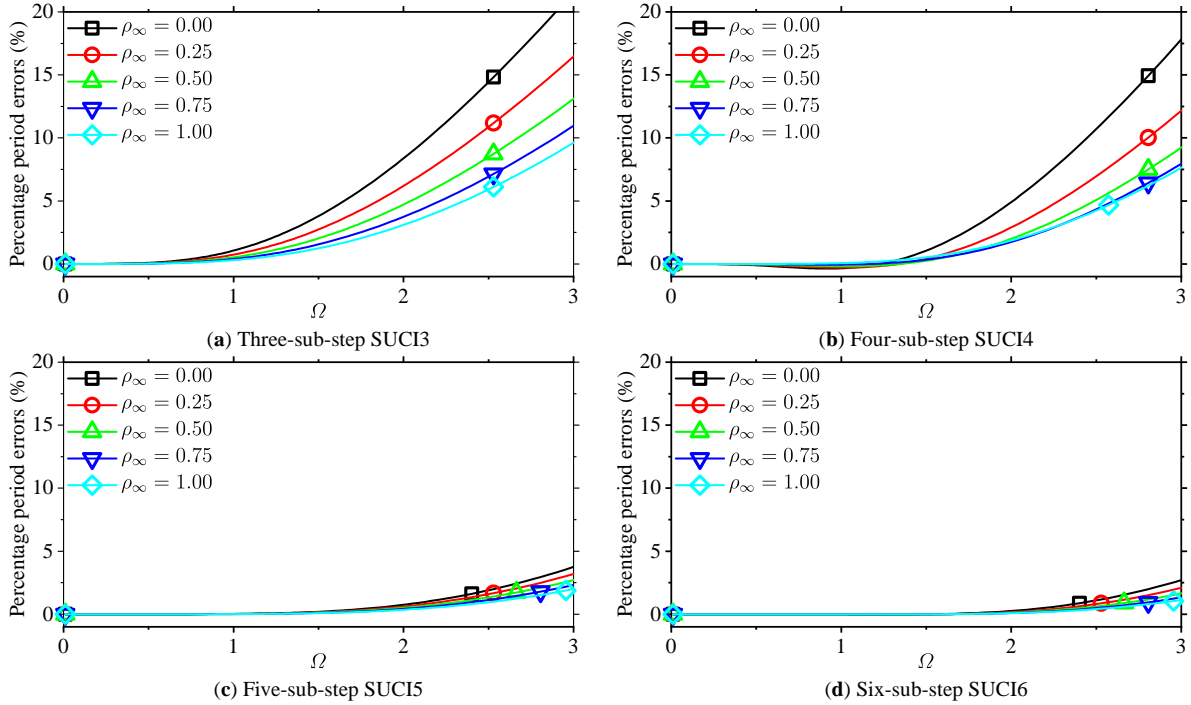


**Fig. 7:** Percentage period errors of four novel high-order integration algorithms in the absence of  $\xi$ .

#### 4.1. Comparisons

Spectral properties of SUCIn have been analyzed and compared with the common second-order schemes such as generalized- $\alpha$  [9, 10] and SUCI2 [18]. Herein, the third-order dissipative EG3 [25] using the extrapolation technique, the third-order  $\rho_\infty$ -Bathe [45, 46] using the four-point load selections, the fourth-order non-dissipative trapezoidal rule (TR-TS) using the Tarnow and Simo technique [26], and the third-order trapezoidal rule (TR-CS) using the complex sub-step strategy [29, 31] are compared with SUCIn. Notice that EG3 can impose slight numerical dissipation via  $\beta_2 = (\rho_\infty - 2 - \sqrt{\rho_\infty^2 + 2\rho_\infty - 2}) / (4\rho_\infty - 4)$  where  $\rho_\infty \in (\sqrt{3} - 1, 1)$  and  $\rho_\infty = 3/4$  is highly recommended in the original study [25] reaching the smallest period errors, while TR-CS employs a complex algorithmic parameter and achieves

controllable numerical dissipation. As with EG3, the third-order  $\rho_\infty$ -Bathe method cannot present a full range of dissipation due to  $\rho_\infty \in (-1, 1 - \sqrt{3}]$  and it attains the minimum period errors at  $\rho_\infty = 1 - \sqrt{3} \approx -0.732$ . In this paper,  $\rho_\infty = -3/4$  is used for the third-order  $\rho_\infty$ -Bathe algorithm since it provides almost the same spectral properties as  $\rho_\infty = 1 - \sqrt{3}$ .

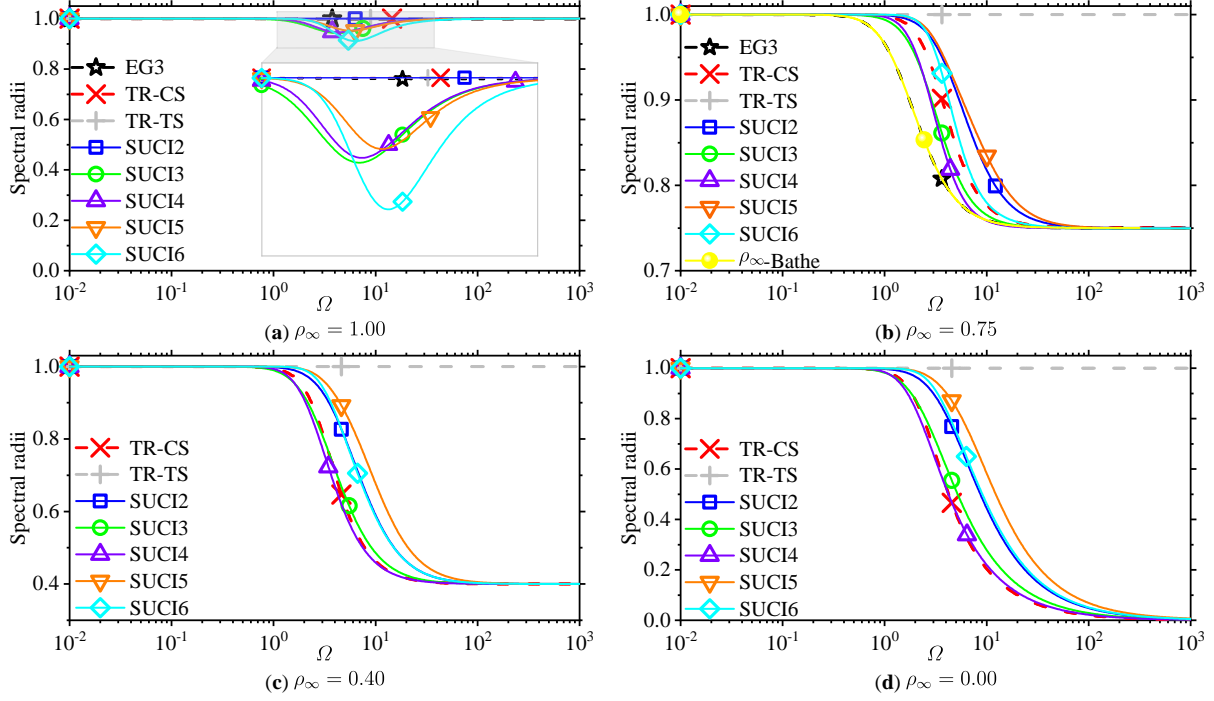


**Fig. 8:** Comparisons of spectral radii among various algorithms when considering different  $\rho_\infty$  in the absence of  $\xi$ . Notice that EG3 [25] uses  $\rho_\infty = 0.999$  in the subplot (a) and  $\rho_\infty$ -Bathe [45] should use the negative value of  $\rho_\infty$  in the subplot (b).

Spectral radii, percentage amplitude decays, and period errors of various integration algorithms with four different values of  $\rho_\infty$  are plotted in Figs. 8-10. Some important observations from these plots are collected as follows.

- In the non-dissipative ( $\rho_\infty = 1$ ) case, four novel high-order integration algorithms produce some amplitude decays in the middle-frequency range, as shown in the subplots (a) of Figs. 8 and 9. In addition, the third-order EG3 scheme [25] only imposes slight dissipation in the high-frequency range due to  $\rho_\infty \in (\sqrt{3} - 1, 1)$ , thus it is not included in the cases of  $\rho_\infty = 0.4$  and  $0.0$ . Similarly, the third-order  $\rho_\infty$ -Bathe algorithm [45] is compared only in the case of  $\rho_\infty = -0.75$ .
- Among the third-order accurate algorithms, EG3 [25] and  $\rho_\infty$ -Bathe [45] provide the worst spectral behavior, such as the largest amplitude decays and period errors in the low-frequency range, while TR-CS [29, 31] produces the better spectral accuracy than SUCI3. However, it will be shown later that TR-CS requires more considerable computational costs than SUCI3 due to involving complex computations. In other words, TR-CS possesses better spectral accuracy at the expense of computational costs.
- For the fourth-order accurate schemes, SUCI4 shows the greater advantage than TR-TS [26] since SUCI4 not only achieves controllable numerical dissipation but also produces significantly fewer period errors.
- Fig. 10 clearly illustrates that within the framework of (2), the higher-order composite multi-sub-step scheme generally provides fewer period errors, so predicting more accurate numerical solutions.

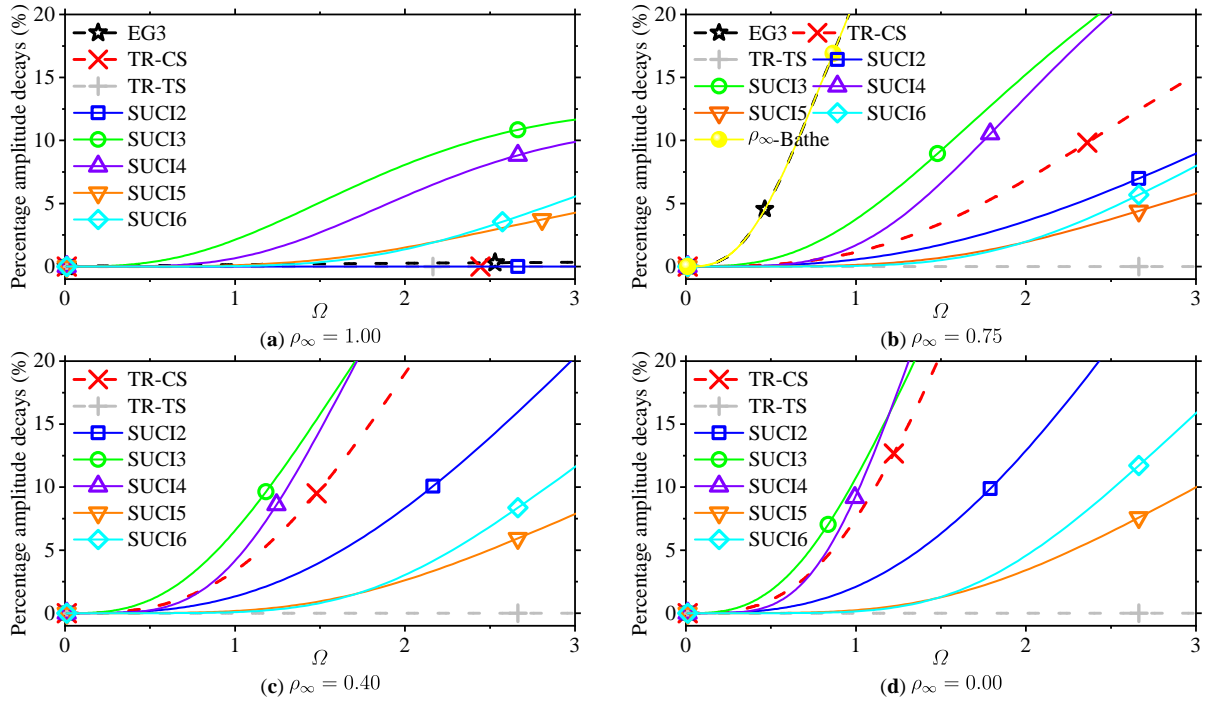


**Fig. 9:** Comparisons of amplitude decays among various algorithms when considering different  $\rho_\infty$  in the absence of  $\xi$ . Notice that EG3 [25] uses  $\rho_\infty = 0.999$  in the subplot (a) and  $\rho_\infty$ -Bathe [45] should use the negative value of  $\rho_\infty$  in the subplot (b).

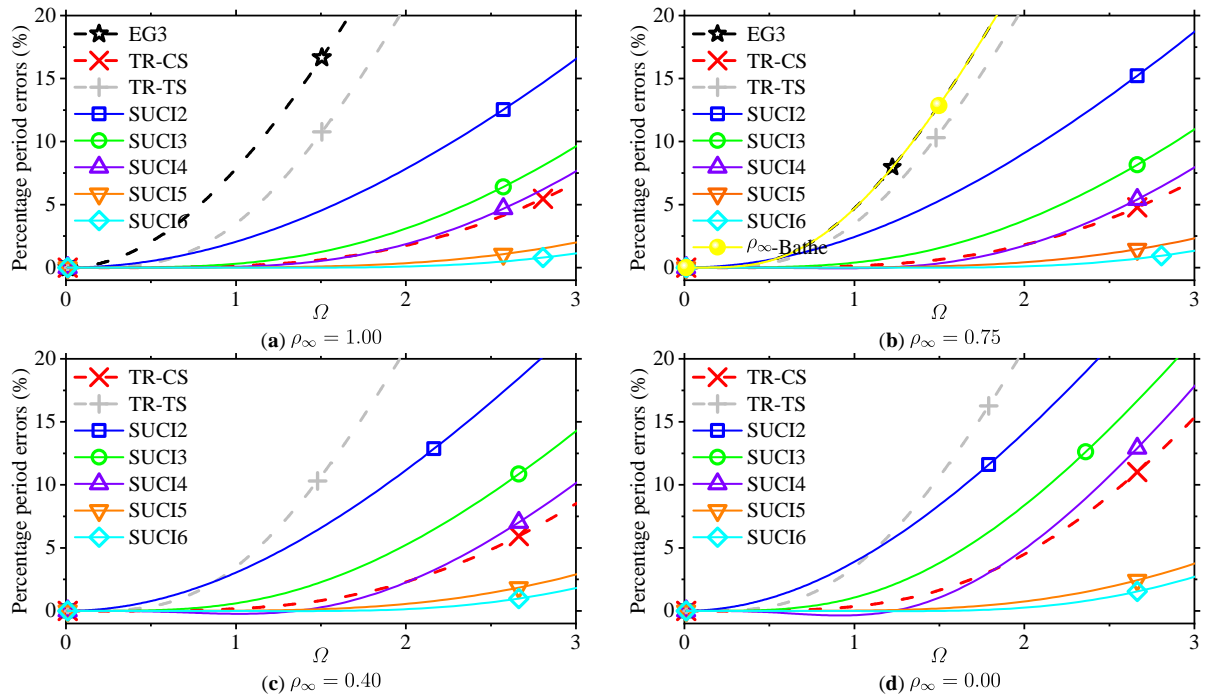


**Fig. 10:** Comparisons of period errors among various algorithms when considering different  $\rho_\infty$  in the absence of  $\xi$ . Notice that EG3 [25] uses  $\rho_\infty = 0.999$  in the subplot (a) and  $\rho_\infty$ -Bathe [45] should use the negative value of  $\rho_\infty$  in the subplot (b).

The directly self-starting high-order implicit methods [35] (DSUCIn) share similar spectral properties with SUCIn developed in this paper. In detail, except for the composite five-sub-step implicit methods, other sub-step methods between DSUCIn and SUCIn present the same spectral properties, and their comparisons are not thus given herein. However, for the composite five-sub-step members, SUCI5 and DSUCI5 [35] provide different spectral properties and their comparisons are plotted in Fig. 11. As one can observe, the proposed SUCI5 method imposes less numerical dissipation and fewer period elongation errors than DSUCI5. Hence, the novel five-sub-step member outperforms DSUCI5 in terms of spectral properties.

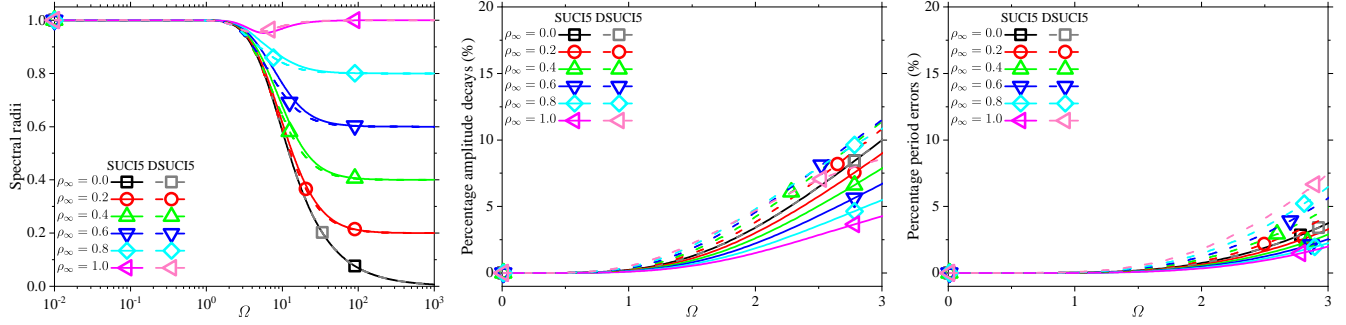


**Fig. 11:** Comparisons of spectral properties between DSUCI5 [35] and SUCI5 in the absence of  $\xi$ .

## 5. Numerical examples

This section will solve some linear and nonlinear examples to demonstrate that

- (a) SUCIn achieves identical designed order of accuracy for solving general structures and does not suffer from the order reduction. For example, SUCI6 provides identical sixth-order accuracy in displacement, velocity, and acceleration for solving the damped forced vibration;
- (b) SUCIn embedding controllable numerical dissipation can not only effectively filter out spurious high-frequency components but also accurately integrate important low-frequency modes;
- (c) SUCIn possesses significant advantages over some published methods for solving nonlinear dynamics, and
- (d) the computational cost of SUCIn is acceptable compared with the published high-order schemes. For instance, the third-order SUCI3 algorithm requires less computational time than the third-order TR-CS scheme [29, 31].

### 5.1. A damped SDOF problem

The damped SDOF system [52] subjected to the nonzero external load is solved to test the numerical accuracy for various integrators used in this paper. It is rigorous for confirming the numerical accuracy to solve the damped forced system. For example, EG3 [25] that achieves third-order accuracy for solving free vibrations is only second-order accurate for simulating forced vibrations. The damped SDOF system is described as

$$\ddot{u}(t) + 4\dot{u}(t) + 5u(t) = \sin(2t) \quad (52)$$

with initial conditions  $u(0) = 57/65$ ,  $\dot{u}(0) = 2/65$ . The exact displacement is calculated as  $u(t) = \exp(-2t)(\cos(t) + 2\sin(t)) - (8\cos(2t) - \sin(2t))/65$ . The global error [53] is computed by using

$$\text{Error} = \left[ \sum_{j=1}^N (x(t_j) - x_j)^2 / \sum_{j=1}^N (x(t_j))^2 \right]^{1/2} \quad (53)$$

where  $N$  denotes the total number of time steps in the analysis;  $x(t_j)$  and  $x_j$  stand for the exact and numerical solutions at time  $t_j$ , respectively. In this test, the total simulation time is assumed to be  $t \approx 5.62$ s.

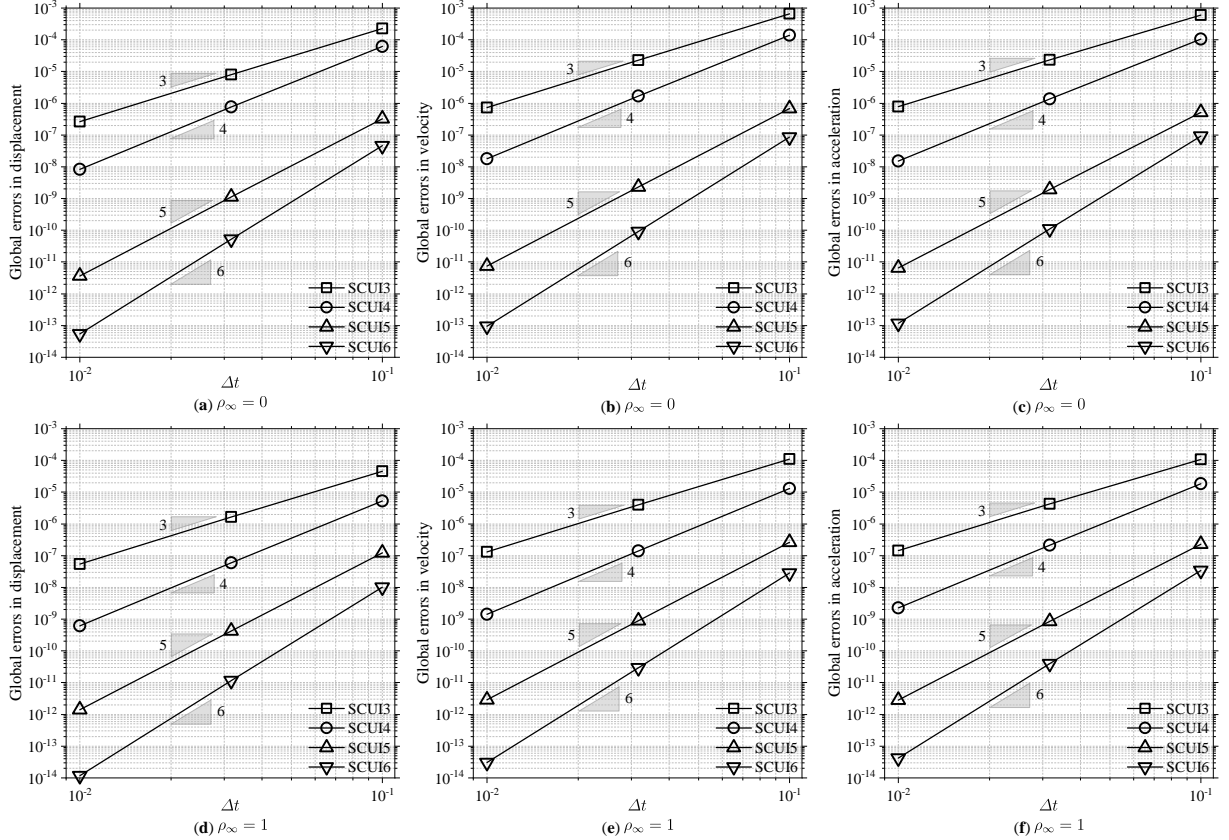


**Fig. 12:** Convergence ratios of four novel high-order SUCIn algorithms: (a-c): $\rho_\infty = 0$  and (d-f):  $\rho_\infty = 1$ .

Fig. 12 first plots global errors in displacement, velocity, and acceleration versus the integration step using SUCIn. It is apparent that four high-order algorithms all achieve their designed orders of accuracy in displacement, velocity, and acceleration. For comparisons, global errors of EG3 [25], TR-CS [29, 31],  $\rho_\infty$ -Bathe [45], and SUCI3 are plotted in Fig. 13, where TR-CS and SUCI3 are obviously superior to EG3 since EG3 presents second-order accuracy for solving forced vibrations. TR-CS produces fewer global errors than SUCI3 due to requiring much more computational costs, while the third-order  $\rho_\infty$ -Bathe presents the largest global errors among all third-order algorithms. Fig. 14 plots global errors of the SDOF system (52) using the fourth-order accurate algorithms. It is obvious that SUCI4 is superior to TR-TS [26] and MSSTH4 [34]. Particularly, MSSTH4 suffers from the order reduction for solving forced vibrations in the non-dissipative case, showing third-order accuracy. This case also holds for MSSTH5 [34]. Hence, the proposed SUCI5 algorithm is obviously superior to MSSTH5.

This damped SDOF system subjected to the nonzero load clearly shows that the proposed high-order algorithms (SUCIn) achieve identical designed order of accuracy in displacement, velocity, and acceleration. Most importantly,

they do not suffer from the order reduction. These conclusions are naturally valid for simulating other simpler cases, such as the undamped and/or free vibrations.

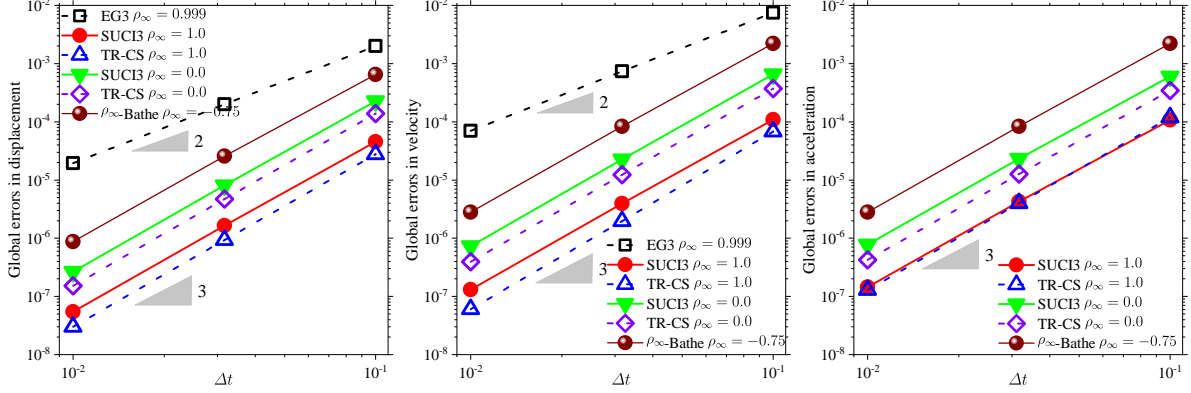


Fig. 13: Comparisons of global errors among the third-order accurate algorithms for solving the damped forced vibration.

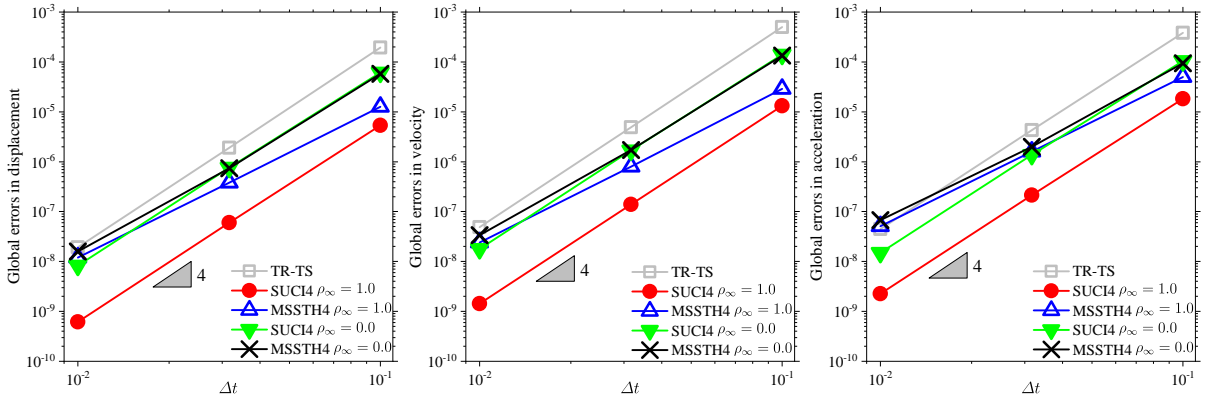


Fig. 14: Comparisons of global errors among the fourth-order accurate algorithms for solving the damped forced vibration.

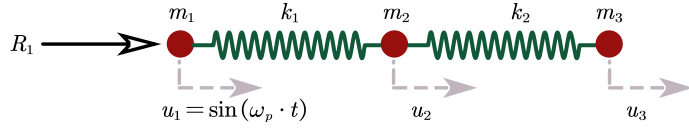


Fig. 15: A linear mass-spring system where  $k_1 = 10^7 \text{ N/m}$ ,  $k_2 = 1 \text{ N/m}$ ,  $m_1 = 0 \text{ kg}$ ,  $m_2 = m_3 = 1 \text{ kg}$ ,  $\omega_p = 1.2 \text{ rad/s}$ .

### 5.2. Double-degree-of-freedom system with spurious high-frequency component

A standard modal problem [16, 54] shown in Fig. 15 has been solved by various dissipative algorithms to show their capabilities of eliminating spurious high-frequency modes. This mass-spring system represents the complex structural dynamic problems, consisting of stiff and flexible parts. The initial governing equation is expressed as

$$\begin{bmatrix} m_1 & 0 & 0 \\ 0 & m_2 & 0 \\ 0 & 0 & m_3 \end{bmatrix} \begin{bmatrix} \ddot{u}_1 \\ \ddot{u}_2 \\ \ddot{u}_3 \end{bmatrix} + \begin{bmatrix} k_1 & -k_1 & 0 \\ -k_1 & k_1 + k_2 & -k_2 \\ 0 & -k_2 & k_2 \end{bmatrix} \begin{bmatrix} u_1 \\ u_2 \\ u_3 \end{bmatrix} = \begin{bmatrix} R_1 \\ 0 \\ 0 \end{bmatrix} \quad (54)$$

where the displacement at node 1 is assumed to be  $u_1 = \sin(\omega_p t) = \sin(1.2t)$  and  $R_1$  is the reaction force at node 1. All initial conditions are set to be zero. By using the known  $u_1$  at node 1, Eq. (54) is further simplified as

$$\begin{bmatrix} m_2 & 0 \\ 0 & m_3 \end{bmatrix} \begin{bmatrix} \ddot{u}_2 \\ \ddot{u}_3 \end{bmatrix} + \begin{bmatrix} k_1 + k_2 & -k_2 \\ -k_2 & k_2 \end{bmatrix} \begin{bmatrix} u_2 \\ u_3 \end{bmatrix} = \begin{bmatrix} k_1 u_1 \\ 0 \end{bmatrix}. \quad (55)$$

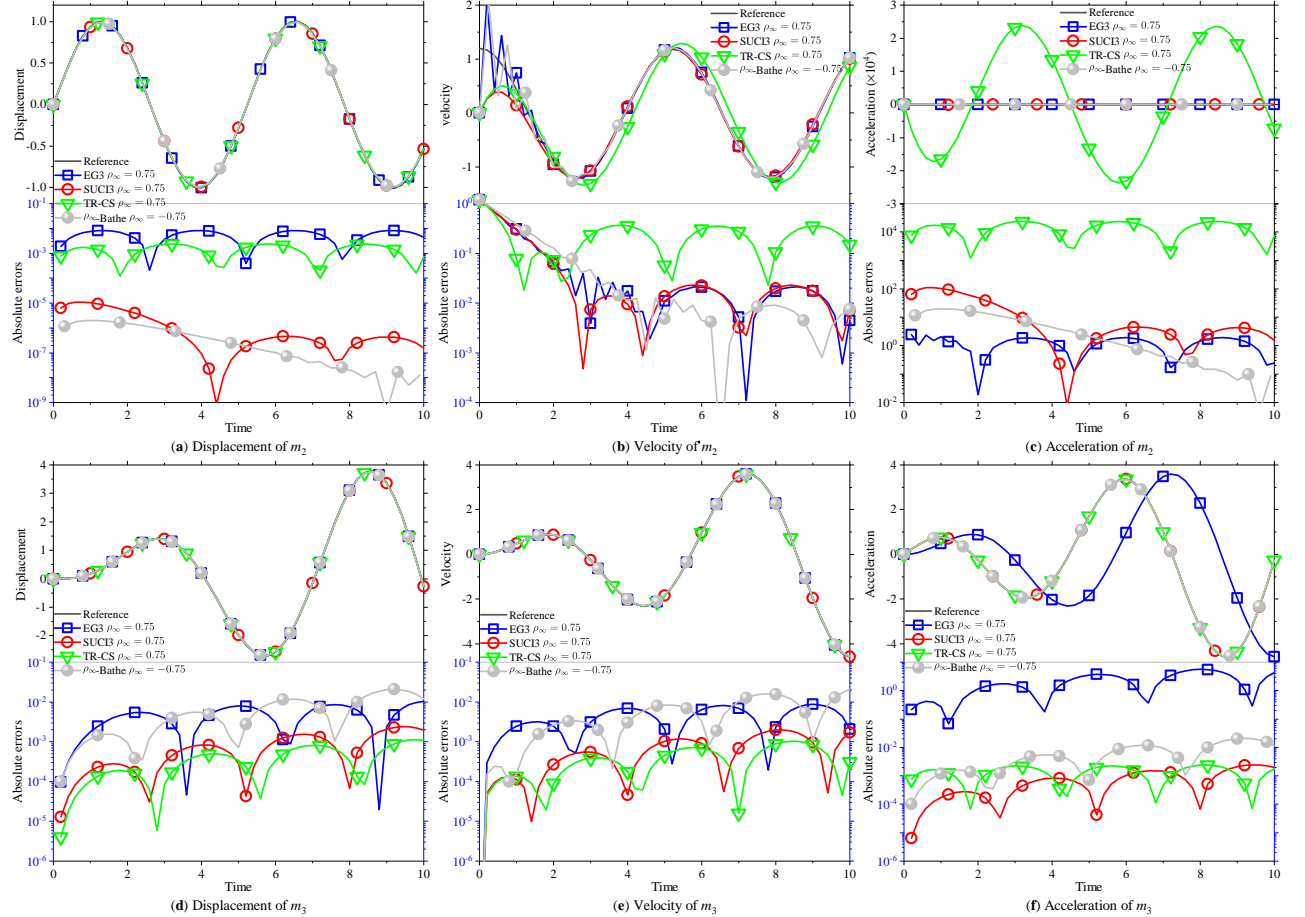


**Fig. 16:** Numerical responses of the mass-spring system using the third-order  $\rho_\infty$ -Bathe [45], EG3 [25], TR-CS [29, 31], and SUCI3 algorithms with the same  $\Delta t = 0.2s$ .

Fig. 16 plots numerical solutions and absolute errors of the mass-spring system by using four third-order accurate algorithms. Considering that EG3 [25] and  $\rho_\infty$ -Bathe [45] can obtain the minimum period errors at  $\rho_\infty = 0.75$  and  $\rho_\infty = -0.75$ , respectively, another two algorithms, namely TR-CS [29, 31] and SUCI3, also use  $\rho_\infty = 0.75$  to ensure the same dissipation in the high-frequency range. Fig. 16 shows that the complex-sub-step TR-CS scheme presents very obvious errors in numerical solutions of  $m_2$ , and that EG3 also performs worse than other methods for predicting numerical responses of  $m_3$ . Although  $\rho_\infty$ -Bathe [45] provides fewer absolute errors in  $m_2$ , the worse numerical results are also observed in  $m_3$ . Overall, the proposed SUCI3 scheme shows its superiority since it not only eliminates spurious high-frequency modes in  $m_2$  but also accurately integrates the low-frequency component in  $m_3$ .

When using the fourth-order accurate algorithms, that is TR-TS [26] (non-dissipative), MSSTH4 [34], and SUCI4, absolute errors in displacement, velocity, and acceleration are plotted in Fig. 17. Due to the non-dissipative property, TR-TS produces adverse numerical errors in  $m_2$  since it cannot filter out any spurious high-frequency components and the maximum errors in  $m_3$  are also found. These numerical results are agreement well with the previous spec-

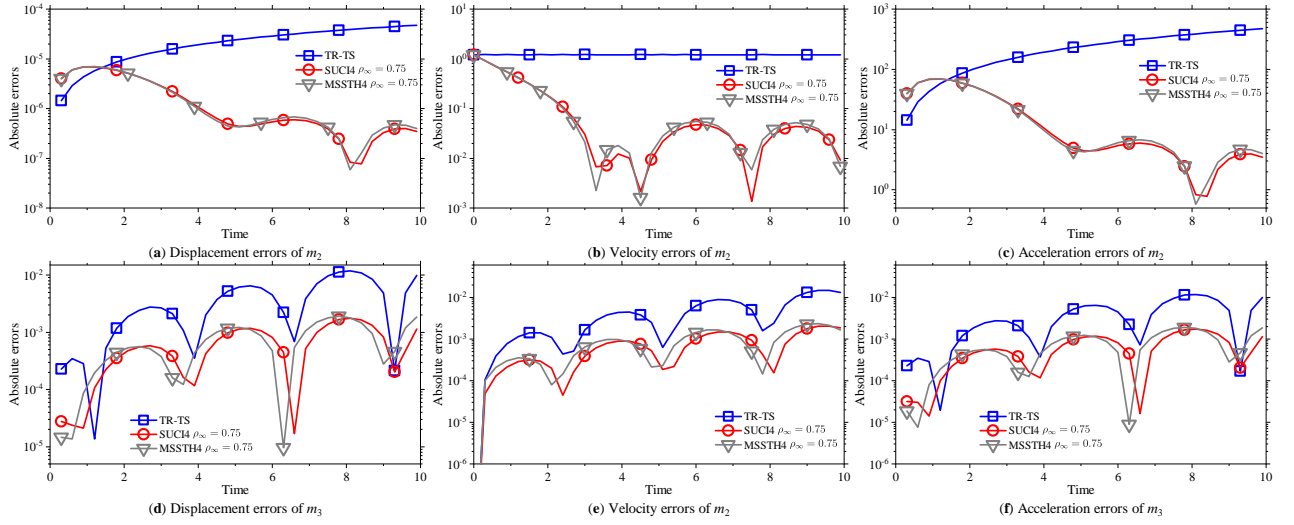


**Fig. 17:** Numerical errors of the mass-spring system using the fourth-order TR-TS (non-dissipative) [26], MSSTH4 [34], and SUCI4 algorithms with the same  $\Delta t = 0.2s$ .

tral analysis in Figs. 8–10. Besides, the proposed SUCI4 algorithm also shows slight advantage over MSSTH4, since the smaller absolute errors are observed for SUCI4. Further considering the higher fifth-order accurate algorithms, namely MSSTH5 [34] and SUCI5, their absolute errors are given in Fig. 18, where the great advantage of SUCI5 over MSSTH5 is shown since the latter has proved to be only third-order accurate for solving forced vibrations [35]. Naturally, the sixth-order accurate SUCI6 scheme can provide more accurate numerical solutions than SUCI5, but these results are not presented herein for brevity.

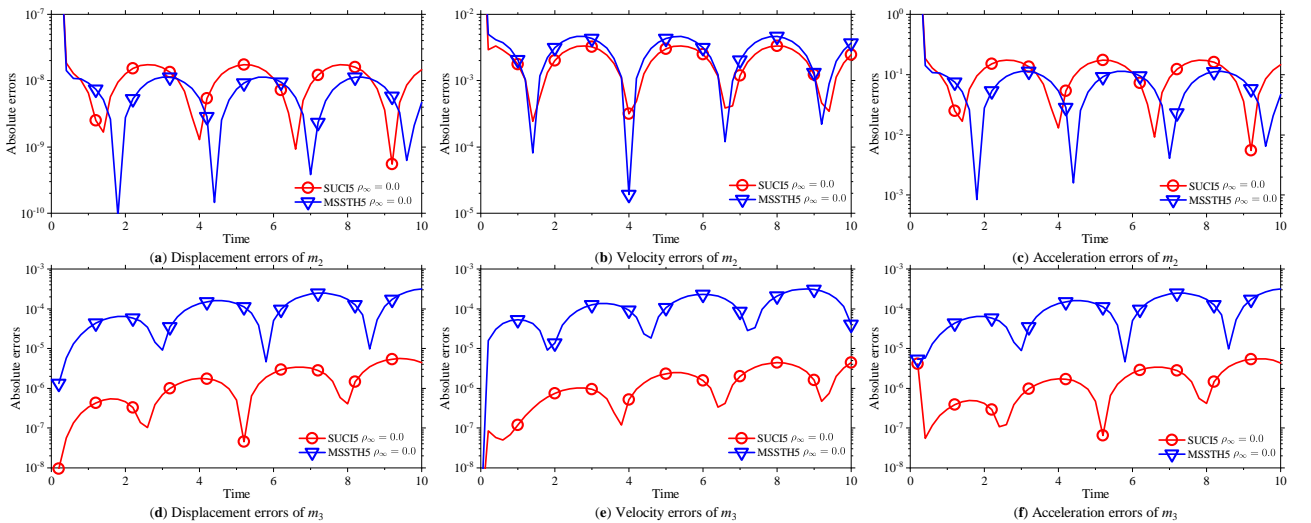


**Fig. 18:** Numerical errors of the mass-spring system using the fifth-order MSSTH5 [34] and SUCI5 algorithms with the same  $\Delta t = 0.2s$ .

This standard double-degree-of-freedom mass-spring system demonstrates that when considering the same order of accuracy, SUCIn can perform better than some existing high-order algorithms with respect to the solution accuracy and dissipation control.

### 5.3. Nonlinear dynamics

This section will solve three nonlinear examples to show the numerical performance of SUCIn on nonlinear dynamics. The classical Newton iteration scheme is used within each (sub-)step and the convergence in equilibrium iterations is reached when one of the following inequalities is satisfied.

$$\|\mathbf{r}^{(i)}\|_2 \leq \text{RTOL} \quad \text{or} \quad \|\Delta \ddot{\mathbf{U}}^{(i)}\|_2 \leq \text{ATOL} \quad (56)$$

where  $\mathbf{r}^{(i)}$  and  $\Delta \ddot{\mathbf{U}}^{(i)}$  are the residuals and increment of the acceleration vector in the  $i$ -th iteration; RTOL and ATOL are two user-specified convergence tolerances and both of them are given as  $1.0 \times 10^{-8}$  in this paper;  $\|\cdot\|_2$  denotes the Euclidean norm, also known as the 2-norm.

#### 5.3.1. A simple pendulum

A classical nonlinear simple pendulum [36] is considered as the first SDOF system with the strong nonlinearity. The governing equation of motion for this pendulum with length  $L = 1\text{m}$  subject to a nonzero initial velocity  $\dot{\theta}_0$  is written as

$$\ddot{\theta}(t) + \frac{g}{L} \sin(\theta(t)) = 0 \quad (57)$$

where  $g$  is the acceleration of gravity and assumed to be unity in this test so that  $g/L = 1$  is satisfied in Eq. (57). It is necessary to point out that  $\dot{\theta}_0 = 1.999999238456499\text{m/s}$  has been widely used to synthesize the highly nonlinear pendulum [36] (*the minimum initial velocity to make the pendulum rotating is calculated as  $\dot{\theta}_{\min} = 2\text{m/s}$* ). In the present case, this simple pendulum should oscillate between two peak points ( $\theta = \pm\pi$ ) instead of making the complete rotation since the initial total energy is slightly less than the minimum total energy to make complete turns.

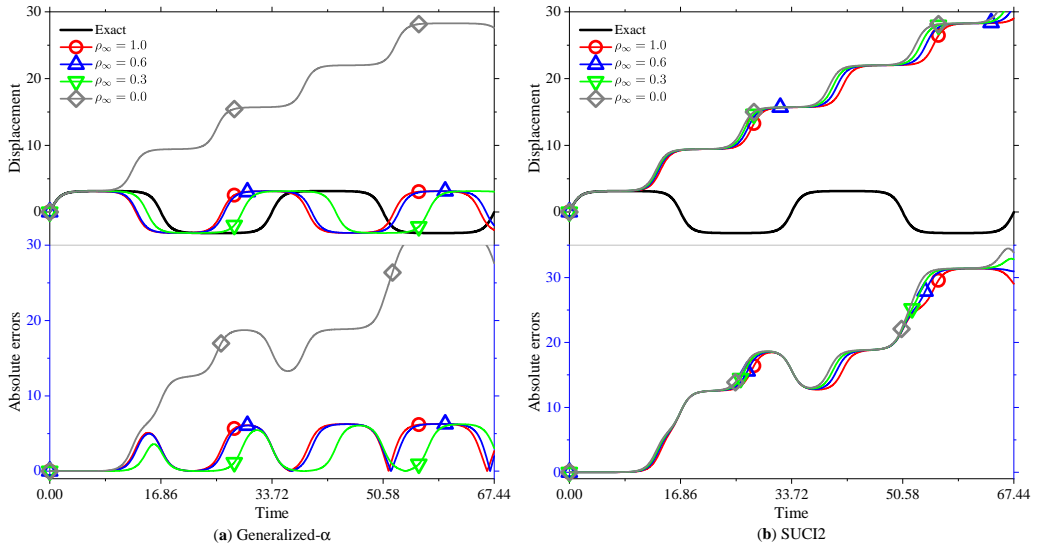


**Fig. 19:** Numerical displacements and absolute errors of the simple pendulum using the generalized- $\alpha$  [9, 10] and SUCI2 [18] algorithms with the same  $\Delta t = 0.02\text{s}$ .

The two second-order accurate algorithms, namely single-step generalized- $\alpha$  [9, 10] and two-sub-step SUCI2 [18], are firstly used to solve this pendulum and their numerical results are presented in Fig. 19. Obviously, using the current time step  $\Delta t = 0.02\text{s}$ , these two algorithms cannot predict reasonable solutions. Particularly, SUCI2 provides the complete turns and generalized- $\alpha$  also presents adverse phase errors. To amplify differences among different

algorithms or parameter settings, Fig. 19 also plots absolute displacement errors, and thus the complete turns make errors tend to infinity with the increase of time.

Next, absolute displacement errors of this simple pendulum using four high-order accurate algorithms (SUCIn) are given in Fig. 20, where two expected facts are revealed. One is that when using the same time step size the higher-order accurate integration algorithms generally perform better than the lower-order ones for solving nonlinear dynamics. It is necessary to point out that such an advantage of high-order algorithms is at the cost of more computational costs and coding complexity. When adopting the integration step size as  $\Delta t = 0.01 \times n$  where  $n$  denotes the number of sub-steps, SUCIn predicts larger absolute errors but still follow the same tendency as those in Fig. 20. The other is that the non-dissipative ( $\rho_\infty = 1$ ) case produces significantly fewer numerical errors than other dissipative cases since there are no spurious high-frequency components in this simple pendulum.

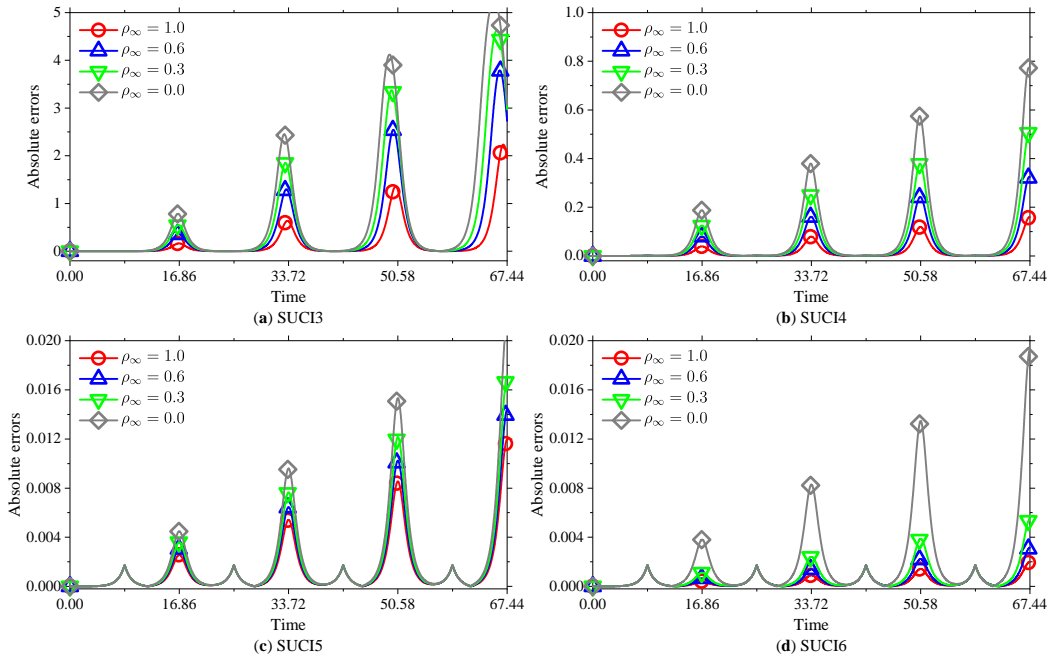


**Fig. 20:** Absolute displacement errors of the simple pendulum using SUCIn with the same  $\Delta t = 0.02s$ .

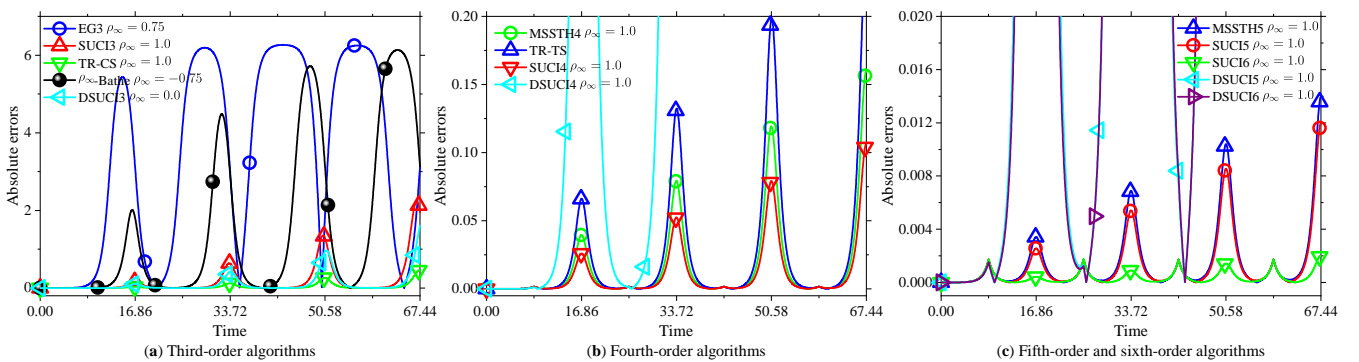


**Fig. 21:** Absolute displacement errors of the simple pendulum using various high-order accurate algorithms with the same  $\Delta t = 0.02s$ .

Finally, comparisons of displacement errors among various high-order accurate algorithms are presented in Fig. 21. Note that each subplot in Fig. 21 adopts the same integration step since they share the same order of accuracy in each subplot. It is apparent that considering the same order of accuracy and integration step, the proposed SUCIn algo-

arithms are significantly superior to the published high-order schemes. For instance, the fourth-order SUCI4 and fifth-order SUCI5 algorithms predict more accurate numerical responses than TR-TS [26], DSUCI(4-6) [35], and MSSTH4/5 [34]. It should be emphasized that although SUCI3 is seemly inferior to TR-CS [29, 31], the latter requires more computational costs due to using the complex algorithmic parameter. In comparison with DSUCIn [35], it is found that DSUCI(4-6) perform worse than other high-order methods in the case of  $\Delta t = 0.02$ s, while DSUCI3 predicts fewer absolute errors than SUCI3. When decreasing the integration step  $\Delta t$  into 0.01s, DSUCIn can also predict quite accurate solutions. Therefore, the present high-order methods are superior to the directly self-starting high-order methods [35] for solving this nonlinear problem since the present methods utilize the acceleration vector  $\ddot{\mathbf{U}}_n$  to obtain more useful information.

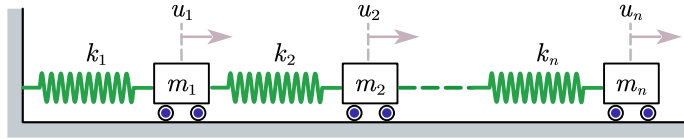


**Fig. 22:** The  $N$ -degree-of-freedom mass-spring model.

### 5.3.2. The $N$ -degree-of-freedom mass-spring system

An  $N$ -degree-of-freedom mass-spring system [52], shown in Fig. 22, is solved to test the computational cost of various integration algorithms. In Fig. 22, all masses are set as  $m_i = 1$ kg, and stiffness coefficients  $k_i$  are assumed as

$$k_i = \begin{cases} k & i = 1 \\ k [1 + \alpha(u_i - u_{i-1})^2] & 2 \leq i \leq N \end{cases} \quad (58)$$

where  $k = 10^5$ N/m and  $\alpha = 2$  is adopted to simulate the nonlinear hardening system. In addition, the model is excited by a force of  $\sin(t)$  for all masses. The completely non-dissipative trapezoidal rule with  $\Delta t = 1.0 \times 10^{-7}$ s is employed to provide reference solutions.

It should be realized that higher-order accurate integration algorithms often require more computational cost than the common second-order ones when the same time step  $\Delta t$  is used. Hence, this example focuses mainly on comparing computational efficiency among the same accurate algorithms. Table 2 firstly records the elapsed computational CPU time and global errors of this mass-spring system with  $N = 1000$ , 5000, and 10000 using the non-dissipative implicit algorithms used in this paper (*the third-order EG3 [25] and  $\rho_\infty$ -Bathe [45] cannot use  $\rho_\infty = \pm 1$  and they are not thus compared herein*). It is evident that when adopting the same integration step  $\Delta t = 0.02$ s, the higher-order integration algorithms need more computational CPU time than the lower-order ones since more sub-steps are used to achieve higher-order accuracy, but these schemes, in turn, produce smaller global errors. As expected, the computational time of each implicit algorithm sharply increases as the degree-of-freedom increases. Notice also that the third-order complex-sub-step TR-CS scheme [29, 31] requires significant more computational time than SUCI3, although it also provides slight smaller global errors. Considering the existing four-sub-step (MSSTH4) and five-sub-step (MSSTH5) schemes [34], it has been shown in [35] that they suffer from the order reduction for solving the forced vibrations. Hence, MSSTH4 and MSSTH5 produce significantly larger global errors than SUCI4 and SUCI5, but almost the same computational time is observed since they use the same number of sub-steps. The fourth-order TR-TS [26] elapses less computational time than MSSTH4 and SUCI4 since it is essentially a composite three-sub-step

Table 2: The elapsed computational time and global errors using the completely non-dissipative ( $\rho_\infty = 1$ ) algorithms.

Algorithms	$\Delta t$	$N = 1000$		$N = 5000$		$N = 10000$	
		CPU time (s)	Global errors	CPU time (s)	Global errors	CPU time (s)	Global errors
Gen.- $\alpha$ [9, 10]	0.02	0.856	$2.3693 \times 10^{-4}$	3.717	$6.9573 \times 10^{-5}$	11.952	$4.7319 \times 10^{-5}$
SUCI2 [18]	0.02	1.213	$6.1301 \times 10^{-5}$	5.975	$1.9814 \times 10^{-5}$	21.248	$1.3714 \times 10^{-5}$
TR-CS [29, 31]	0.02	2.195	$2.3159 \times 10^{-7}$	12.153	$4.2864 \times 10^{-8}$	34.097	$1.3736 \times 10^{-8}$
DSUCI3 [35]	0.02	1.569	$7.5232 \times 10^{-7}$	9.523	$8.6127 \times 10^{-8}$	27.159	$7.0891 \times 10^{-8}$
SUCI3	0.02	1.573	$7.6711 \times 10^{-7}$	9.935	$8.7909 \times 10^{-8}$	27.927	$7.0679 \times 10^{-8}$
TR-TS [26]	0.02	2.021	$3.1656 \times 10^{-7}$	10.265	$5.2774 \times 10^{-8}$	28.086	$1.7341 \times 10^{-8}$
MSSTH4 [34]	0.02	3.044	$2.3373 \times 10^{-7}$	15.836	$3.9261 \times 10^{-8}$	33.098	$9.7313 \times 10^{-9}$
DSUCI4 [35]	0.02	2.993	$1.2882 \times 10^{-7}$	14.273	$2.1149 \times 10^{-8}$	33.108	$3.3021 \times 10^{-9}$
SUCI4	0.02	3.121	$1.3047 \times 10^{-7}$	14.929	$2.1416 \times 10^{-8}$	33.597	$3.3267 \times 10^{-9}$
MSSTH5 [34]	0.02	4.232	$4.8580 \times 10^{-7}$	16.557	$1.0683 \times 10^{-8}$	45.706	$3.3453 \times 10^{-8}$
DSUCI5 [35]	0.02	3.997	$4.3207 \times 10^{-8}$	16.893	$7.2260 \times 10^{-9}$	48.891	$4.3192 \times 10^{-9}$
SUCI5	0.02	3.782	$4.0110 \times 10^{-8}$	16.499	$6.5481 \times 10^{-9}$	47.538	$2.1996 \times 10^{-9}$
DSUCI6 [35]	0.02	4.980	$2.0359 \times 10^{-8}$	22.002	$3.3719 \times 10^{-9}$	70.942	$4.1389 \times 10^{-10}$
SUCI6	0.02	5.133	$2.0897 \times 10^{-8}$	21.155	$3.3846 \times 10^{-9}$	70.707	$4.1463 \times 10^{-10}$

scheme. The directly self-starting high-order algorithms [35] (DSUCIn) show almost the same numerical performance as SUCIn since they share similar numerical characteristics. The most significant difference between DSUCIn and SUCIn is that DSUCIn is designed to be directly self-starting, and thus the acceleration output is additionally constructed. It should be pointed out that the computational CPU time of the high-order  $s$ -sub-step methods, including the published schemes [26, 29, 31, 34, 35], is  $s$  times less than the single-step generalized- $\alpha$ 's [9, 10] computational time. One of the reasons for such the numerical behavior is that the generalized- $\alpha$  method only achieves first-order accurate accelerations, so slowing down convergence speeds.

When considering the most dissipative ( $\rho_\infty = 0$ ) case, the elapsed computational time and global errors among various dissipative algorithms are listed in Table 3. The same conclusions as Table 2 can be concluded. Besides, it is also found that when imposing numerical dissipation in the high-frequency range, larger global errors are produced for these integration algorithms. This observation is well agreement with the spectral analysis in Section 4, where period errors increase as the parameter  $\rho_\infty$  decreases from unity into zero, as shown Figs. 6 and 7.

Tables 2 and 3 mainly compare the numerical performance of high-order implicit methods with the same order of accuracy and the same integration step size. It is interesting to compare the numerical performance among various implicit methods with the same sub-step size. Table 4 records the elapsed computational time and global errors using various algorithms ( $\rho_\infty = 0.0$ ) with the same sub-step size. Note that each implicit method in Table 4 adopts the integration step size  $\Delta t = 0.02 \times s$  to guarantee each sub-step size as 0.02s. With such parameter settings, all implicit methods in Table 4 should elapse almost the same computational time for solving linear structures. However, this is not the case for solving nonlinear problems. As one can observe in Table 4, the composite multi-sub-step methods are significantly superior to the traditional single-step generalized- $\alpha$  [9, 10] method in terms of the computational time and solution accuracy. When the multi-sub-step methods achieve high-order accuracy, such an advantage is further

Table 3: The elapsed computational time and global errors using the most dissipative ( $\rho_\infty = 0$ ) algorithms.

Algorithms	$\Delta t$	$N = 1000$		$N = 5000$		$N = 10000$	
		CPU time (s)	Global errors	CPU time (s)	Global errors	CPU time (s)	Global errors
Gen.- $\alpha$ [9, 10]	0.02	0.810	$1.2973 \times 10^{-3}$	8.062	$3.8377 \times 10^{-4}$	12.797	$2.4291 \times 10^{-4}$
SUCI2 [18]	0.02	1.306	$1.1864 \times 10^{-4}$	12.618	$3.8427 \times 10^{-5}$	20.352	$2.6614 \times 10^{-5}$
TR-CS [29, 31]	0.02	3.058	$2.5343 \times 10^{-6}$	15.455	$4.7898 \times 10^{-7}$	40.748	$1.9784 \times 10^{-7}$
DSUCI3 [35]	0.02	2.231	$4.3721 \times 10^{-6}$	10.231	$8.3518 \times 10^{-7}$	30.191	$3.4987 \times 10^{-7}$
SUCI3	0.02	2.207	$4.3874 \times 10^{-6}$	10.645	$8.3989 \times 10^{-7}$	30.848	$3.5654 \times 10^{-7}$
MSSTH4 [34]	0.02	3.132	$3.3477 \times 10^{-6}$	17.290	$5.2566 \times 10^{-7}$	43.115	$9.4042 \times 10^{-8}$
DSUCI4 [35]	0.02	3.204	$1.3111 \times 10^{-6}$	17.541	$2.2489 \times 10^{-7}$	43.815	$3.4101 \times 10^{-8}$
SUCI4	0.02	3.259	$1.3474 \times 10^{-6}$	17.603	$2.2565 \times 10^{-7}$	43.741	$3.3932 \times 10^{-8}$
MSSTH5 [34]	0.02	4.337	$7.4887 \times 10^{-7}$	21.877	$2.4608 \times 10^{-8}$	57.162	$4.6910 \times 10^{-8}$
DSUCI5 [35]	0.02	4.298	$6.8381 \times 10^{-8}$	20.839	$3.1109 \times 10^{-9}$	57.479	$3.7719 \times 10^{-9}$
SUCI5	0.02	4.375	$6.8380 \times 10^{-8}$	21.161	$3.1171 \times 10^{-9}$	57.565	$3.7500 \times 10^{-9}$
DSUCI6 [35]	0.02	5.012	$4.6142 \times 10^{-8}$	26.997	$7.5503 \times 10^{-9}$	77.212	$7.4311 \times 10^{-10}$
SUCI6	0.02	5.039	$4.5919 \times 10^{-8}$	27.439	$7.4504 \times 10^{-9}$	77.612	$7.2195 \times 10^{-10}$

enhanced. As the number of DOFs increases, various composite implicit methods with the same sub-step size elapse the approximately same CPU time, such as the case of  $N = 10000$ . In addition, some useful conclusions from Tables 2 and 3 are still valid. For instance, the proposed SUCIn method still outperforms MSSTHn [34] since the latter produces larger global errors due to the order reduction for solving forced vibrations.

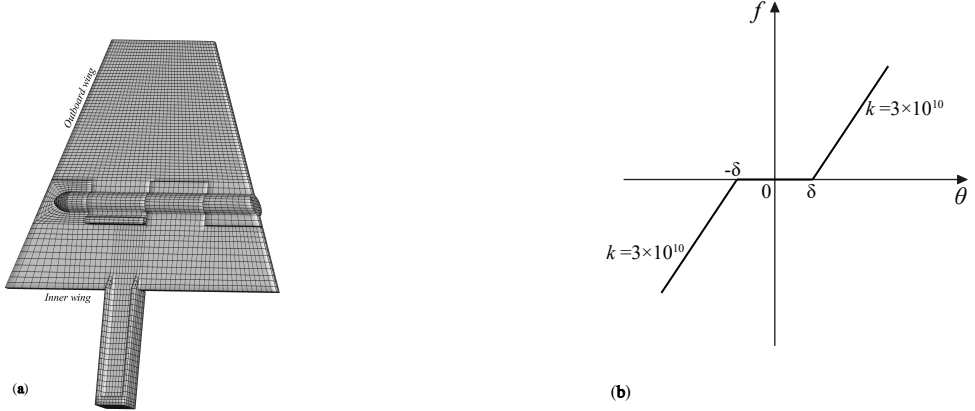


Fig. 23: (a) Finite element model of the folding wing with free-play nonlinearity, and (b) model of the nonlinear torsional spring with  $\delta = 0.1\text{mm}$ .

### 5.3.3. A folding wing with free-play nonlinearity

To further test the numerical performance of SUCIn on the practical engineering problems, a folding wing [21, 55] with free-play nonlinearity consisting of the outboard and inner wings shown in Fig. 23a is solved by various high-order implicit methods. The connection of two wings has been modeled by three same nonlinear torsional springs [55] (see Fig. 23b). The detailed mathematical model of this folding wing can refer to the literature [55]. In this finite element model, there are 9627 solid elements and 80800 DOFs. The initial displacements and velocities of all DOFs are

Table 4: The elapsed computational time and global errors using various algorithms ( $\rho_\infty = 0.0$ ) with the same sub-step size.

Algorithms	$\Delta t$	$N = 1000$		$N = 5000$		$N = 10000$	
		CPU time (s)	Global errors	CPU time (s)	Global errors	CPU time (s)	Global errors
Gen.- $\alpha$ [9, 10]	0.02	0.810	$1.2973 \times 10^{-3}$	8.062	$3.8377 \times 10^{-4}$	12.797	$2.4291 \times 10^{-4}$
SUCI2 [18]	0.04	0.894	$4.7066 \times 10^{-4}$	5.112	$1.5328 \times 10^{-4}$	8.251	$1.0640 \times 10^{-4}$
TR-CS [29, 31]	0.06	0.551	$4.7977 \times 10^{-5}$	5.830	$9.8774 \times 10^{-6}$	8.856	$4.6496 \times 10^{-6}$
DSUCI3 [35]	0.06	0.635	$8.2892 \times 10^{-5}$	5.012	$1.7344 \times 10^{-5}$	8.555	$8.4964 \times 10^{-6}$
SUCI3	0.06	0.640	$8.3278 \times 10^{-5}$	5.131	$1.7509 \times 10^{-5}$	8.519	$8.4836 \times 10^{-6}$
MSSTH4 [34]	0.08	0.691	$6.5893 \times 10^{-5}$	5.422	$4.1022 \times 10^{-5}$	8.073	$6.2424 \times 10^{-6}$
DSUCI4 [35]	0.08	0.681	$6.3889 \times 10^{-5}$	5.515	$1.0912 \times 10^{-5}$	8.478	$3.9765 \times 10^{-6}$
SUCI4	0.08	0.679	$6.3938 \times 10^{-5}$	5.428	$1.1061 \times 10^{-5}$	8.113	$4.1018 \times 10^{-6}$
MSSTH5 [34]	0.10	0.706	$9.2543 \times 10^{-6}$	6.331	$3.7125 \times 10^{-6}$	8.373	$5.6442 \times 10^{-7}$
DSUCI5 [35]	0.10	0.740	$7.2882 \times 10^{-6}$	6.853	$1.1921 \times 10^{-6}$	8.607	$3.9446 \times 10^{-7}$
SUCI5	0.10	0.719	$7.2879 \times 10^{-6}$	6.708	$1.1921 \times 10^{-6}$	8.653	$3.9450 \times 10^{-7}$
DSUCI6 [35]	0.12	0.811	$6.9486 \times 10^{-6}$	7.304	$9.4334 \times 10^{-7}$	9.188	$3.2105 \times 10^{-7}$
SUCI6	0.12	0.813	$6.9481 \times 10^{-6}$	7.297	$9.4433 \times 10^{-7}$	9.180	$3.1510 \times 10^{-7}$

assumed to be zero except that three torsional springs possess the nonzero velocity (20mm/s) to make the outboard and inner wings meet with each other.

Numerical angle displacements of the third torsional spring using the high-order integration algorithms are plotted in Fig. 24, where the reference solutions are obtained by using the sixth-order accurate SUCI6 scheme with a smaller time step  $\Delta t = 1.0 \times 10^{-7}$ s. It follows that the third-order complex-sub-step TR-CS scheme [29, 31] produces adverse phase errors compared with SUCI3, EG3 [25], and  $\rho_\infty$ -Bathe [45]. Moreover, other SUCIn schemes in Fig. 24b-d also show better robustness than MSSTHn [34] and TR-TS [26]. DSUCI4 [35] and DSUCI5 [35] perform better than SUCI4 and SUCI5, respectively, in the present settings. As emphasized previously, except for the acceleration output, the previous DSUCIn [35] method possesses comparative numerical performance with SUCIn. On the other hand, this nonlinear example does not strictly follow the previous experience that when using the same integration step size the higher-order schemes can generally predict more accurate numerical responses than the lower-order ones. For instance, the third-order SUCI3( $\rho_\infty = 0$ ) and sixth-order SUCI6( $\rho_\infty = 0$ ) methods perform better than other schemes for solving the present problem.

In practical applications, users often need to simulate the analyzed structure more than once via selecting different integration algorithms, algorithmic parameters, and time steps. Based on the spectral analysis in Section 4 and numerical results in this section, the proposed SUCIn schemes are highly recommended for solving various dynamical problems in priority.

## 6. Conclusions

This paper constructs a general composite  $s$ -sub-step implicit scheme (2) for second-order hyperbolic problems. Via the accuracy and dissipation analysis, four novel high-order implicit algorithms (SUCIn) are developed to achieve the following numerical characteristics.

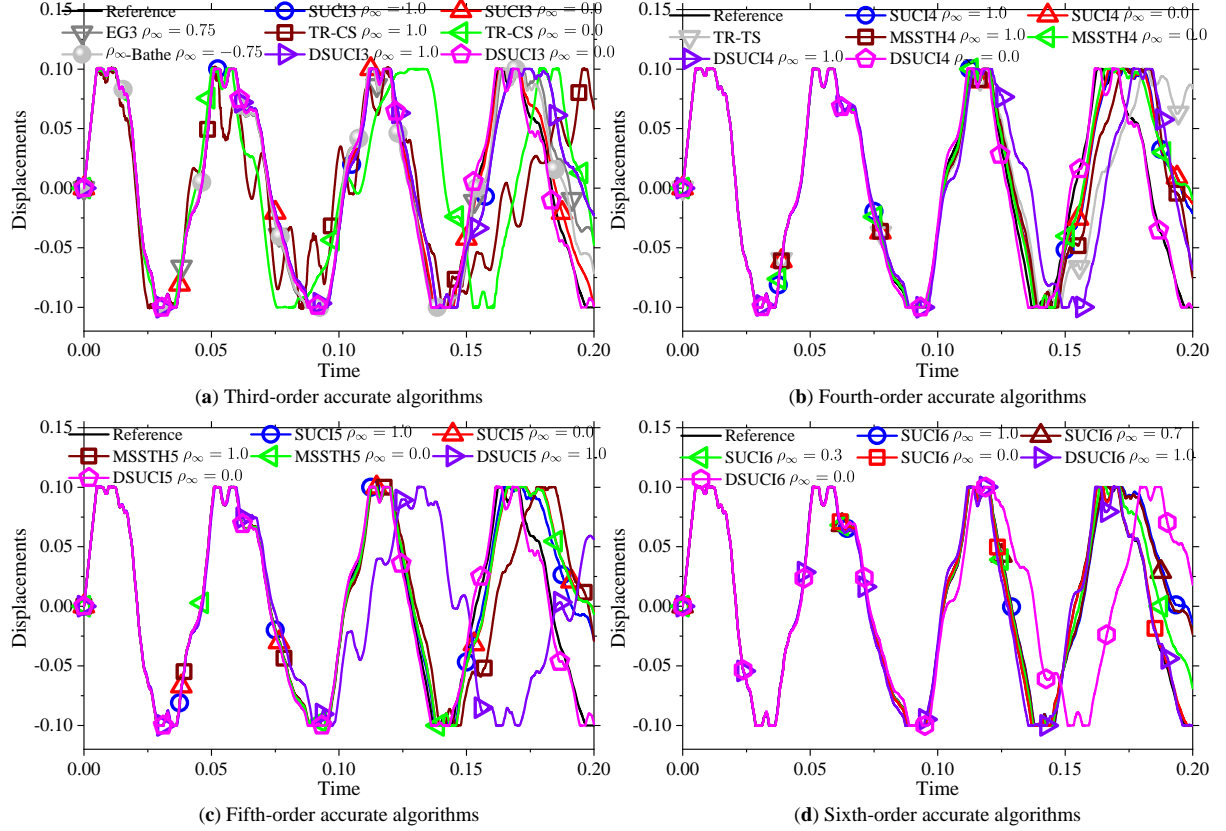


**Fig. 24:** Numerical angle displacements of the third torsional spring using the high-order integration algorithms with the same  $\Delta t = 2.5 \times 10^{-5}$ s.

- (a) Four novel methods are higher-order accurate and avoid the order reduction for solving forced vibrations. The analysis reveals that the  $s$ -sub-step implicit scheme (2) can achieve  $s$ th-order accuracy in the case of  $2 \leq s \leq 6$ ; otherwise it needs more sub-steps to achieve higher-order accuracy when embedding dissipation control and unconditional stability. Hence, this paper only develops four cost-optimal high-order methods corresponding to three, four, five, and six sub-steps.
- (b) Four novel methods can control numerical dissipation in the high-frequency range by changing  $\rho_\infty \in [0, 1]$ , so effectively eliminating spurious high-frequency components when accurately integrating important low-frequency modes.
- (c) Four novel methods achieve identical effective stiffness matrices within each sub-step. Many studies have shown that this property can not only effectively save the computational cost for solving linear structures but also produce optimal spectral properties, namely the maximum dissipation but minimum period errors.

Apart from these, SUCIn also possesses some primary numerical properties. For instance, the unconditional stability is ensured during the process of achieving controllable numerical dissipation, which is also confirmed in the spectral analysis. In addition, the third-order consistency within each sub-step is required and the trapezoidal rule has to thus be employed in their first sub-steps. Of course, four novel methods are naturally self-starting and do not suffer from overshoots.

Numerical examples are solved to confirm the numerical performance and advantages of SUCIn. Two typical but straightforward linear systems, namely a standard SDOF damped system subjected to the external force and a double-

degree-of-freedom mass-spring model with the spurious high-frequency mode, are solved to test the numerical accuracy and dissipation control of SUCIn. SUCIn and the published schemes are used to solve three nonlinear problems. When adopting the same integration step size, the higher-order methods are generally superior to the lower-order ones with respect to solving nonlinear dynamics. In contrast, when considering the same order of accuracy and computational costs, four novel methods perform better than the published high-order schemes.

## Acknowledgments

This work is supported by the National Natural Science Foundation of China (Grant No. 12102103 and 12272105), the Heilongjiang Touyan Innovation Team Program, and Fundamental Research Funds for the Central Universities (Grant No. HIT.NSRIF.2020014). In addition, the first author acknowledges the financial support by the China Scholarship Council (Grant No. 202006120104).

## Conflict of interest

The authors declare that they have no known competing financial interests or personal relationships that could have appeared to influence the work reported in this paper.

## Data availability

Data sharing not applicable to this article as no datasets were generated or analyzed during the current study.

## Appendix A: Six-sub-step sixth-order scheme: SUCI6

In this appendix, the six-sub-step implicit algorithm is developed. Numerical schemes in the first four sub-steps are the same as those of SUCI5, and numerical schemes in the last two sub-steps are explicitly written as follows.

$$\mathbf{M}\ddot{\mathbf{U}}_{n+\gamma_5} + \mathbf{C}\dot{\mathbf{U}}_{n+\gamma_5} + \mathbf{K}\mathbf{U}_{n+\gamma_5} = \mathbf{F}(t_n + \gamma_5\Delta t)$$

$$\mathbf{M}\ddot{\mathbf{U}}_{n+1} + \mathbf{C}\dot{\mathbf{U}}_{n+1} + \mathbf{K}\mathbf{U}_{n+1} = \mathbf{F}(t_{n+1}) \quad (A1a)$$

$$\mathbf{U}_{n+\gamma_5} = \mathbf{U}_n + \Delta t \left( \sum_{j=0}^4 \alpha_{5j} \dot{\mathbf{U}}_{n+\gamma_j} + \frac{\gamma_1}{2} \ddot{\mathbf{U}}_{n+\gamma_5} \right)$$

$$\mathbf{U}_{n+1} = \mathbf{U}_n + \Delta t \left( \sum_{j=0}^5 \alpha_{6j} \dot{\mathbf{U}}_{n+\gamma_j} + \frac{\gamma_1}{2} \ddot{\mathbf{U}}_{n+1} \right) \quad (A1b)$$

$$\dot{\mathbf{U}}_{n+\gamma_5} = \dot{\mathbf{U}}_n + \Delta t \left( \sum_{j=0}^4 \alpha_{5j} \ddot{\mathbf{U}}_{n+\gamma_j} + \frac{\gamma_1}{2} \dddot{\mathbf{U}}_{n+\gamma_5} \right)$$

$$\dot{\mathbf{U}}_{n+1} = \dot{\mathbf{U}}_n + \Delta t \left( \sum_{j=0}^5 \alpha_{6j} \ddot{\mathbf{U}}_{n+\gamma_j} + \frac{\gamma_1}{2} \dddot{\mathbf{U}}_{n+1} \right) \quad (A1c)$$

Notice that the above scheme has achieved identical effective stiffness matrices within each sub-step. The conditions (19) achieving sixth-order accuracy, as well as additional constraints (22), are used to determine  $\alpha_{ij}$ , which are

$$\alpha_{20} = \frac{-\gamma_1^2 + 3\gamma_1\gamma_2 - \gamma_2^2}{2\gamma_1}$$

$$\alpha_{21} = \frac{\gamma_2(\gamma_2 - \gamma_1)}{2\gamma_1} \quad (A2a)$$

$$\alpha_{30} = \frac{-\gamma_1^2 + (3\gamma_3 - 2\alpha_{32})\gamma_1 + 2\alpha_{32}\gamma_2 - \gamma_3^2}{2\gamma_1}$$

$$\alpha_{31} = \frac{-2\alpha_{32}\gamma_2 - \gamma_1\gamma_3 + \gamma_3^2}{2\gamma_1} \quad (A2b)$$

$$\alpha_{40} = \frac{-\gamma_1^2 + (3\gamma_4 - 2\alpha_{42} - 2\alpha_{43})\gamma_1 + 2\alpha_{42}\gamma_2 + 2\alpha_{43}\gamma_3 - \gamma_4^2}{2\gamma_1}$$

$$\alpha_{41} = \frac{-2\alpha_{42}\gamma_2 - 2\alpha_{43}\gamma_3 - \gamma_1\gamma_4 + \gamma_4^2}{2\gamma_1} \quad (A2c)$$

$$\alpha_{50} = \frac{-\gamma_1^2 + (3\gamma_5 - 2\alpha_{52} - 2\alpha_{53} - 2\alpha_{54})\gamma_1 + 2\alpha_{52}\gamma_2 + 2\alpha_{53}\gamma_3 + 2\alpha_{54}\gamma_4 - \gamma_5^2}{2\gamma_1} \quad (A2d)$$

$$\alpha_{51} = \frac{-2\alpha_{52}\gamma_2 - 2\alpha_{53}\gamma_3 - 2\alpha_{54}\gamma_4 - \gamma_1\gamma_5 + \gamma_5^2}{2\gamma_1} \quad (\text{A2e})$$

$$\alpha_{60} = \frac{-\gamma_1^2 + (3 - 2\alpha_{62} - 2\alpha_{63} - 2\alpha_{64} - 2\alpha_{65})\gamma_1 + 2\alpha_{62}\gamma_2 + 2\alpha_{63}\gamma_3 + 2\alpha_{64}\gamma_4 + 2\alpha_{65}\gamma_5 - 1}{2\gamma_1} \quad (\text{A2f})$$

$$\alpha_{61} = \frac{-2\alpha_{62}\gamma_2 - 2\alpha_{63}\gamma_3 - 2\alpha_{64}\gamma_4 - 2\alpha_{65}\gamma_5 - \gamma_1 + 1}{2\gamma_1} \quad (\text{A2g})$$

$$\alpha_{32} = \frac{45\gamma_1^5 - 225\gamma_1^4 + 300\gamma_1^3 - 150\gamma_1^2 + 30\gamma_1 - 2}{720\alpha_{65}\alpha_{54}\alpha_{43}\gamma_2(\gamma_1 - \gamma_2)} \quad (\text{A2h})$$

$$\alpha_{42} = \frac{\left\{ \begin{array}{l} -45(\alpha_{64}\alpha_{43} + \alpha_{65}\alpha_{53})\gamma_1^5 + (225\alpha_{64}\alpha_{43} + 225\alpha_{65}\alpha_{53} - 90\alpha_{65}\alpha_{54}\alpha_{43})\gamma_1^4 + 720\alpha_{65}^2\alpha_{54}^2\alpha_{43}^2\gamma_3^2 \\ + (360\alpha_{65}\alpha_{54}\alpha_{43} - 300\alpha_{64}\alpha_{43} - 300\alpha_{65}\alpha_{53})\gamma_1^3 + (150\alpha_{64}\alpha_{43} + 150\alpha_{65}\alpha_{53} - 360\alpha_{65}\alpha_{54}\alpha_{43})\gamma_1^2 \\ + (120\alpha_{65}\alpha_{54}\alpha_{43} - 30\alpha_{64}\alpha_{43} - 30\alpha_{65}\alpha_{53} - 720\alpha_{65}^2\alpha_{54}^2\alpha_{43}^2\gamma_3)\gamma_1 - 12\alpha_{65}\alpha_{54}\alpha_{43} + 2\alpha_{64}\alpha_{43} + 2\alpha_{65}\alpha_{53} \end{array} \right\}}{720\alpha_{65}^2\alpha_{54}^2\alpha_{43}\gamma_2(\gamma_1 - \gamma_2)} \quad (\text{A2i})$$

$$\alpha_{52} = \frac{\left\{ \begin{array}{l} 45(\alpha_{64}^2\alpha_{43} + \alpha_{65}\alpha_{64}\alpha_{53} - \alpha_{65}\alpha_{63}\alpha_{54})\gamma_1^5 - 12\alpha_{65}\alpha_{54}\alpha_{43}(5\alpha_{65}\alpha_{54} - \alpha_{64}) + 2\alpha_{65}(\alpha_{63}\alpha_{54} - \alpha_{64}\alpha_{53}) \\ + (90\alpha_{65}\alpha_{64}\alpha_{54}\alpha_{43} - 225\alpha_{64}^2\alpha_{43} - 225\alpha_{65}\alpha_{64}\alpha_{53} + 225\alpha_{65}\alpha_{63}\alpha_{54})\gamma_1^4 + 720\alpha_{65}^3\alpha_{54}^2\alpha_{43}(\alpha_{54}\gamma_4^2 + \alpha_{53}\gamma_3^2) \\ + [180\alpha_{65}\alpha_{54}\alpha_{43}(\alpha_{65}\alpha_{54} - 2\alpha_{64}) + 300(\alpha_{64}^2\alpha_{43} + \alpha_{65}\alpha_{64}\alpha_{53} - \alpha_{65}\alpha_{63}\alpha_{54})]\gamma_1^3 - 2\alpha_{43}\alpha_{64}^2 \\ + [180\alpha_{65}\alpha_{54}\alpha_{43}(2\alpha_{64} - 3\alpha_{65}\alpha_{54}) - 150(\alpha_{64}^2\alpha_{43} + \alpha_{65}\alpha_{64}\alpha_{53} - \alpha_{65}\alpha_{63}\alpha_{54})]\gamma_1^2 \\ + [360\alpha_{65}^2\alpha_{54}^2\alpha_{43}(1 - 2\alpha_{65}(\alpha_{54}\gamma_4 + \alpha_{53}\gamma_3)) - 30\alpha_{64}\alpha_{43}(4\alpha_{65}\alpha_{54} - \alpha_{64}) + 30\alpha_{65}(\alpha_{64}\alpha_{53} - \alpha_{63}\alpha_{54})]\gamma_1 \end{array} \right\}}{720\alpha_{65}^3\alpha_{54}^2\alpha_{43}\gamma_2(\gamma_1 - \gamma_2)} \quad (\text{A2j})$$

$$\alpha_{62} = \frac{6\alpha_{63}\gamma_3(\gamma_1 - \gamma_3) + 6\alpha_{64}\gamma_4(\gamma_1 - \gamma_4) + 6\alpha_{65}\gamma_5(\gamma_1 - \gamma_5) + 3\gamma_1^2 - 6\gamma_1 + 2}{6\gamma_2(\gamma_2 - \gamma_1)} \quad (\text{A2k})$$

$$\alpha_{43} = \frac{\left\{ \begin{array}{l} 60\alpha_{65}\alpha_{53}\gamma_3(\gamma_2 - \gamma_3)(\gamma_3 - \gamma_1) + 60\alpha_{65}\alpha_{54}\gamma_4(\gamma_2 - \gamma_4)(\gamma_4 - \gamma_1) + 5\gamma_1^2(3\gamma_1\gamma_2 - 3\gamma_1 - 9\gamma_2 + 7) \\ + 30\gamma_1\gamma_2 - 20\gamma_1 - 5\gamma_2 + 3 \end{array} \right\}}{60\alpha_{64}\gamma_3(\gamma_2 - \gamma_3)(\gamma_1 - \gamma_3)} \quad (\text{A2l})$$

$$\alpha_{53} = \frac{\left\{ \begin{array}{l} 240\alpha_{65}^2\alpha_{54}^2\gamma_4(\gamma_2 - \gamma_4)(\gamma_4 - \gamma_1) + 30\alpha_{64}\gamma_1^4(\gamma_2 - 1) + [60\alpha_{65}\alpha_{54}(\gamma_2 - 1) + 30\alpha_{64}(3 - 4\gamma_2)]\gamma_1^3 \\ + [20\alpha_{65}\alpha_{54}(7 - 9\gamma_2) + 15\alpha_{64}(8\gamma_2 - 5)]\gamma_1^2 + [40\alpha_{65}\alpha_{54}(3\gamma_2 - 2) + 2\alpha_{64}(11 - 20\gamma_2)]\gamma_1 \\ + 4\alpha_{65}\alpha_{54}(3 - 5\gamma_2) + 2\alpha_{64}(2\gamma_2 - 1) \end{array} \right\}}{240\alpha_{65}^2\alpha_{54}\gamma_3(\gamma_2 - \gamma_3)(\gamma_1 - \gamma_3)} \quad (\text{A2m})$$

$$\alpha_{63} = \frac{12\alpha_{64}\gamma_4(\gamma_2 - \gamma_4)(\gamma_4 - \gamma_1) + 12\alpha_{65}\gamma_5(\gamma_2 - \gamma_5)(\gamma_5 - \gamma_1) - 6\gamma_1(\gamma_1(\gamma_2 - 1) - 2\gamma_2) - 10\gamma_1 - 4\gamma_2 + 3}{12\gamma_3(\gamma_2 - \gamma_3)(\gamma_1 - \gamma_3)} \quad (\text{A2n})$$

$$\alpha_{54} = \frac{\left\{ \begin{array}{l} 15(\gamma_3 - 1)(\gamma_2 - 1)\gamma_1^3 + [35\gamma_3 - 30 + 5\gamma_2(7 - 9\gamma_3)]\gamma_1^2 + [15 - 20\gamma_3 + 10\gamma_2(3\gamma_3 - 2)]\gamma_1 \\ + (3 - 5\gamma_3)\gamma_2 + 3\gamma_3 - 2 \end{array} \right\}}{60\alpha_{65}\gamma_4(\gamma_3 - \gamma_4)(\gamma_2 - \gamma_4)(\gamma_1 - \gamma_4)} \quad (\text{A2o})$$

$$\alpha_{64} = \frac{\left\{ \begin{array}{l} 30(1 - \gamma_3)(\gamma_2 - 1)\gamma_1^2 + [45 - 50\gamma_3 + 10\gamma_2(6\gamma_3 - 5) - 60\alpha_{65}\gamma_5(\gamma_3 - \gamma_5)(\gamma_2 - \gamma_5)]\gamma_1 \\ + [15 - 20\gamma_3 + 60\alpha_{65}\gamma_5^2(\gamma_3 - \gamma_5)]\gamma_2 - 60\alpha_{65}\gamma_5^3(\gamma_3 - \gamma_5) + 15\gamma_3 - 12 \end{array} \right\}}{60\gamma_4(\gamma_3 - \gamma_4)(\gamma_2 - \gamma_4)(\gamma_1 - \gamma_4)} \quad (\text{A2p})$$

$$\alpha_{65} = \frac{\left\{ \begin{array}{l} 30(1 - \gamma_4)(\gamma_3 - 1)(\gamma_2 - 1)\gamma_1^2 + (45 - 50\gamma_4 + 10\gamma_3(6\gamma_4 - 5))\gamma_1\gamma_2 + 3\gamma_3(5\gamma_4 - 4) \\ + (45\gamma_4 - 42 + 5\gamma_3(9 - 10\gamma_4))\gamma_1 + (15\gamma_4 - 12 + 5\gamma_3(3 - 4\gamma_4))\gamma_2 - 12\gamma_4 + 10 \end{array} \right\}}{60\gamma_5(\gamma_4 - \gamma_5)(\gamma_3 - \gamma_5)(\gamma_2 - \gamma_5)(\gamma_1 - \gamma_5)} \quad (\text{A2q})$$

The remaining algorithmic parameters are only five splitting ratios of sub-step size, namely  $\gamma_i$  ( $i = 1, \dots, 5$ ). Like

the previous composite sub-step methods, the first splitting ratio  $\gamma_1$  is given to control numerical dissipation in the high-frequency range. In the high-frequency limit  $\omega \rightarrow \infty$ , the characteristic polynomial (25) is simplified as

$$\left( \zeta_\infty - \frac{45\gamma_1^6 - 540\gamma_1^5 + 1350\gamma_1^4 - 1200\gamma_1^3 + 450\gamma_1^2 - 72\gamma_1 + 4}{45\gamma_1^6} \right)^2 = 0. \quad (\text{A3})$$

Then, the controllably dissipative conditions (27) require

$$\frac{45\gamma_1^6 - 540\gamma_1^5 + 1350\gamma_1^4 - 1200\gamma_1^3 + 450\gamma_1^2 - 72\gamma_1 + 4}{45\gamma_1^6} = \rho_\infty. \quad (\text{A4})$$

Obviously, it is almost impossible in Eq. (A4) to obtain the analytical expression of  $\gamma_1$  with respect to  $\rho_\infty$ . Hence, the useful numerical relations are also given in Table 1. Other splitting ratios  $\gamma_i$  ( $i = 2, \dots, 5$ ) are taken by default as  $\gamma_i = i \cdot \gamma_1$  ( $i = 2, \dots, 5$ ) in this paper.

## References

- [1] T. J. R. Hughes, The Finite Element Method: Linear Static and Dynamic Finite Element Analysis, Dover Civil and Mechanical Engineering, Dover Publications, 2000.
- [2] J. Li, K. Yu, X. Li, An identical second-order single step explicit integration algorithm with dissipation control for structural dynamics, *International Journal for Numerical Methods in Engineering* 122 (4) (2021) 1089–1132.
- [3] G. Noh, K.-J. Bathe, An explicit time integration scheme for the analysis of wave propagations, *Computers & Structures* 129 (2013) 178–193.
- [4] J. Li, K. Yu, R. Zhao, Two third-order explicit integration algorithms with controllable numerical dissipation for second-order nonlinear dynamics, *Computer Methods in Applied Mechanics and Engineering* 395 (2022) 114945.
- [5] N. M. Newmark, A method of computation for structural dynamics, *Journal of Engineering Mechanic Division* 85 (3) (1959) 67–94.
- [6] E. L. Wilson, I. Farhoomand, K. J. Bathe, Nonlinear dynamic analysis of complex structures, *Earthquake Engineering & Structural Dynamics* 1 (3) (1972) 241–252.
- [7] H. M. Hilber, T. J. R. Hughes, R. L. Taylor, Improved numerical dissipation for time integration algorithms in structural dynamics, *Earthquake Engineering & Structural Dynamics* 5 (3) (1977) 283–292.
- [8] W. Wood, M. Bossak, O. Zienkiewicz, An alpha modification of Newmark's method, *International Journal for Numerical Methods in Engineering* 15 (10) (1980) 1562–1566.
- [9] H. Shao, C. Cai, A three parameters algorithm for numerical integration of structural dynamic equations, *Chinese Journal of Applied Mechanics* 5 (4) (1988) 76–81.
- [10] J. Chung, G. M. Hulbert, A time integration algorithm for structural dynamics with improved numerical dissipation: The generalized- $\alpha$  method, *Journal of Applied Mechanics* 60 (2) (1993) 371–375.
- [11] K. J. Bathe, M. M. I. Baig, On a composite implicit time integration procedure for nonlinear dynamics, *Computers & Structures* 83 (31–32) (2005) 2513–2524.
- [12] K. J. Bathe, Conserving energy and momentum in nonlinear dynamics: A simple implicit time integration scheme, *Computers & Structures* 85 (7–8) (2007) 437–445.
- [13] J. Li, X. Li, K. Yu, Enhanced studies on the composite sub-step algorithm for structural dynamics: The Bathe-like algorithm, *Applied Mathematical Modelling* 80 (2020) 33–64.
- [14] J. Li, K. Yu, H. Tang, Further assessment of three Bathe algorithms and implementations for wave propagation problems, *International Journal of Structural Stability and Dynamics* 21 (5) (2021) 2150073.
- [15] G. Noh, K.-J. Bathe, The Bathe time integration method with controllable spectral radius: The  $\rho_\infty$ -Bathe method, *Computers & Structures* 212 (2019) 299–310.
- [16] J. Li, K. Yu, X. Li, A novel family of controllably dissipative composite integration algorithms for structural dynamic analysis, *Nonlinear Dynamics* 96 (4) (2019) 2475–2507.
- [17] M. Rezaiee-Pajand, S. R. Sarafrazi, A mixed and multi-step higher-order implicit time integration family, *Archive Proceedings of the Institution of Mechanical Engineers Part C Journal of Mechanical Engineering Science* 224 (10) (2010) 2097–2108.
- [18] J. Li, K. Yu, A novel family of composite sub-step algorithms with desired numerical dissipations for structural dynamics, *Archive of Applied Mechanics* 90 (4) (2020) 737–772.

[19] S. Dong, BDF-like methods for nonlinear dynamic analysis, *Journal of Computational Physics* 229 (8) (2010) 3019–3045.

[20] J. Li, K. Yu, An alternative to the Bathe algorithm, *Applied Mathematical Modelling* 69 (2019) 255–272.

[21] J. Li, K. Yu, A truly self-starting implicit family of integration algorithms with dissipation control for nonlinear dynamics, *Nonlinear Dynamics* 102 (4) (2020) 2503–2530.

[22] J. Li, K. Yu, A simple truly self-starting and L-stable integration algorithm for structural dynamics, *International Journal of Applied Mechanics* 12 (10) (2020) 1–29.

[23] M. M. Malakiyah, S. Shojaee, K.-J. Bathe, The Bathe time integration method revisited for prescribing desired numerical dissipation, *Computers & Structures* 212 (2019) 289–298.

[24] Y. Ji, Y. Xing, An optimized three-sub-step composite time integration method with controllable numerical dissipation, *Computers & Structures* 231 (2020) 106210.

[25] T. Fung, S. Fan, G. Sheng, Extrapolated Galerkin time finite elements, *Computational Mechanics* 17 (6) (1996) 398–405.

[26] N. Tarnow, J. C. Simo, How to render second order accurate time-stepping algorithms fourth order accurate while retaining the stability and conservation properties, *Computer Methods in Applied Mechanics and Engineering* 115 (3) (1994) 233–252.

[27] T. Fung, Unconditionally stable higher-order accurate hermitian time finite elements, *International Journal for Numerical Methods in Engineering* 39 (20) (1996) 3475–3495.

[28] W. Kim, J. N. Reddy, Effective Higher-Order Time Integration Algorithms for the Analysis of Linear Structural Dynamics, *Journal of Applied Mechanics* 84 (7) (2017) 071009.

[29] T. Fung, Unconditionally stable higher-order Newmark methods by sub-stepping procedure, *Computer Methods in Applied Mechanics and Engineering* 147 (1-2) (1997) 61–84.

[30] S. Fan, T. Fung, G. Sheng, A comprehensive unified set of single-step algorithms with controllable dissipation for dynamics .1. Formulation, *Computer Methods in Applied Mechanics and Engineering* 145 (1-2) (1997) 87–98.

[31] T. C. Fung, Complex-time-step Newmark methods with controllable numerical dissipation, *International Journal for Numerical Methods in Engineering* 41 (1) (1998) 65–93.

[32] M. Mancuso, F. Ubertini, An efficient integration procedure for linear dynamics based on a time discontinuous Galerkin formulation, *Computational Mechanics* 32 (3) (2003) 154–168.

[33] S. Krenk, Conservative fourth-order time integration of non-linear dynamic systems, *Computer Methods in Applied Mechanics and Engineering* 295 (2015) 39–55.

[34] H. Zhang, R. Zhang, Y. Xing, P. Maserati, On the optimization of n-sub-step composite time integration methods, *Nonlinear Dynamics* 102 (3) (2020) 1939–1962.

[35] J. Li, R. Zhao, K. Yu, X. Li, Directly self-starting higher-order implicit integration algorithms with flexible dissipation control for structural dynamics, *Computer Methods in Applied Mechanics and Engineering* 389 (2022) 114274.

[36] W. Kim, J. N. Reddy, A new family of higher-order time integration algorithms for the analysis of structural dynamics, *Journal of Applied Mechanics* 84 (7) (2017) 071008–17.

[37] Y. Wang, K. Tamma, D. Maxam, T. Xue, G. Qin, An Overview of High-Order Implicit Algorithms for First-/Second-Order Systems and Novel Explicit Algorithm Designs for First-Order System Representations, *Archives of Computational Methods in Engineering* (2021).

[38] T. C. Fung, Weighting parameters for unconditionally stable higher-order accurate time step integration algorithms. Part 2-second-order equations (1999) 36.

[39] A. V. Idesman, A new high-order accurate continuous Galerkin method for linear elastodynamics problems, *Computational Mechanics* 40 (2) (2007) 261–279.

[40] J. H. Argyris, P. C. Dunne, T. Angelopoulos, Dynamic response by large step integration, *Earthquake Engineering & Structural Dynamics* 2 (2) (1973) 185–203.

[41] X. Li, N. Wiberg, Structural dynamic analysis by a time-discontinuous Galerkin finite element method, *International Journal for Numerical Methods in Engineering* 39 (12) (1996) 2131–2152.

[42] J. de Frutos, J. M. Sanz-Serna, An easily implementable fourth-order method for the time integration of wave problems, *Journal of Computational Physics* 103 (1) (1992) 160–168.

[43] C. Song, S. Eisenträger, X. Zhang, High-order implicit time integration scheme based on Padé expansions, *Computer Methods in Applied Mechanics and Engineering* 390 (2022) 114436.

[44] D. Soares, A straightforward high-order accurate time-marching procedure for dynamic analyses, *Engineering with Computers* 38 (2022) 1659–1677.

[45] S.-B. Kwon, K.-J. Bathe, G. Noh, Selecting the load at the intermediate time point of the  $\rho_\infty$ -Bathe time integration scheme, *Computers & Structures* 254 (2021) 106559.

[46] B. Choi, K.-J. Bathe, G. Noh, Time splitting ratio in the  $\rho_\infty$ -bathe time integration method for higher-order accuracy in structural dynamics and heat transfer, *Computers & Structures* 270 (2022) 106814.

[47] M. Rezaiee-Pajand, S. R. Sarafrazi, M. Hashemian, Improving stability domains of the implicit higher order accuracy method, *International Journal for Numerical Methods in Engineering* 88 (9) (2011) 880–896.

[48] M. Rezaiee-Pajand, M. Hashemian, A. Bohluly, A novel time integration formulation for nonlinear dynamic analysis, *Aerospace Science & Technology* 69 (2017) 625–635.

[49] M. Rezaiee-Pajand, S. A. H. Esfehani, H. Ehsanmanesh, An efficient weighted residual time integration family, *International Journal of Structural Stability and Dynamics* 21 (8) (2021) 2150106.

[50] K. Yu, A new family of generalized- $\alpha$  time integration algorithms without overshoot for structural dynamics, *Earthquake Engineering & Structural Dynamics* 37 (12) (2008) 1389–1409.

[51] S. Klarmann, W. Wagner, Enhanced studies on a composite time integration scheme in linear and non-linear dynamics, *Computational Mechanics* 55 (3) (2015) 455–468.

[52] J. Li, K. Yu, X. Li, A generalized structure-dependent semi-explicit method for structural dynamics, *Journal of Computational and Nonlinear Dynamics* 13 (11) (2018) 20.

[53] D. Soares Jr, A simple and effective new family of time marching procedures for dynamics, *Computer Methods in Applied Mechanics & Engineering* 283 (2014) 1138–1166.

[54] K.-J. Bathe, G. Noh, Insight into an implicit time integration scheme for structural dynamics, *Computers & Structures* 98–99 (2012) 1–6.

[55] H. He, H. Tang, K. Yu, J. Li, N. Yang, X. Zhang, Nonlinear aeroelastic analysis of the folding fin with freeplay under thermal environment, *Chinese Journal of Aeronautics* 33 (9) (2020) 2357–2371.